C. R. Mecanique 339 (2011) 532–551

Contents lists available at ScienceDirect

Comptes Rendus Mecanique

www.sciencedirect.com

Surface mechanics: facts and numerical models

Experimental and numerical analysis of fretting crack formation based on 3D X-FEM frictional contact fatigue crack model

Simulation expérimentale et numérique X-FEM de fissures tridimensionnelles de fatigue avec contact et frottement. Application au fretting

Emilien Pierres, Marie-Christine Baietto *, Anthony Gravouil

INSA-Lyon, LaMCoS, CNRS UMR5259, bâtiment Jean-d'Alembert, 18, 20, rue des Sciences, 69621 Villeurbanne cedex, France

ARTICLE INFO

Article history:
Available online 21 June 2011

Keywords:
X-FEM
Fatigue
Fretting
Frictional contact

Mots-clés :
X-FEM
Fatigue
Fretting
Contact frottement

ABSTRACT

Nowadays, numerical simulation of 3D fatigue crack growth is easily handled using the eXtended Finite Element Method coupled with level set techniques. The finite element mesh does not need to conform to the crack geometry. Most difficulties associated to complex mesh generation around the crack and the re-meshing steps during the possible propagation are hence avoided. A 3D two-scale frictional contact fatigue crack model developed within the X-FEM framework is presented in this article. It allows the use of a refined discretization of the crack interface independent from the underlying finite element mesh and adapted to the frictional contact crack scale. A stabilized three-field weak formulation is also proposed to avoid possible oscillations in the local solution linked to the LBB condition when tangential slip is occurring. Two basic three-dimensional numerical examples are presented. They aim at illustrating the capacities and the high level of accuracy of the proposed X-FEM model. Stress intensity factors are computed along the crack front. Finally an experimental 3D ball/plate fretting fatigue test with running conditions inducing crack nucleation and propagation is modeled. 3D crack shapes defined from actual experimental ones and fretting loading cycle are considered. This latter numerical simulation demonstrates the model ability to deal with challenging actual complex problems and the possibility to achieve tribological fatigue prediction at a design stage based on the fatigue crack modeling.

RÉSUMÉ

De nos jours, la méthode des éléments finis étendus couplée aux techniques de fonctions de niveau (level-set) a été appliquée avec succès à un grand nombre d'applications et en particulier à la simulation de la propagation de fissures de fatigue tridimensionnelles. En effet, la géométrie de la fissure ne doit pas être maillée explicitement. La plupart des difficultés liées à la génération de maillages complexes autour de la fissure et les opérations de re-maillage et de projection de champs lors de la propagation sont donc évitées. Un modèle 3D à deux échelles, celle de la structure et celle de de la fissure, développé dans le cadre X-FEM est présenté dans ce papier. Il permet l'utilisation d'une discrétisation raffinée de l'interface de la fissure, adaptée à l'échelle des non linéarités de contact avec frottement et indépendante du maillage éléments finis sous-jacent. Une formulation faible stabilisée à trois champs est également proposée afin d'éviter les oscillations possibles

* Corresponding author.
E-mail addresses: emilien.pierres@insa-lyon.fr (E. Pierres), marie-christine.baietto@insa-lyon.fr (M.-C. Baietto), anthony.gravouil@insa-lyon.fr (A. Gravouil).

1631-0721/$ – see front matter
doi:10.1016/j.crme.2011.05.011

dans la solution locale liées à la condition LBB en cas de glissement tangentiel. Deux exemples numériques simples en trois dimensions sont présentés. Ils visent à illustrer les capacités et le niveau élevé de précision du modèle X-FEM proposé. Enfin, le modèle est intégré dans une démarche globale couplant expérimenation et simulation numérique pour prédire la durée de vie de composants en fatigue. Des essais de fretting menés pour des conditions de chargement induisant l'initiation et la propagation de fissures sont simulés numériquement. Les conditions de chargement et les faciès de fissuration 3D sont utilisés comme données d'entrée dans le modèle numérique X-FEM. Les conditions de contact et frottement à l'interafce des fissures sont déterminées au cours d'un cycle de fretting et les facteurs d'intensité de contraintes en mode I, II et III sont calculés. Cette simulation démontre la capacité de modèle à faire face aux défis posés par les problèmes réels complexes et la possibilité de réaliser une prédiction en fatigue tribologique des composants de structures.

1. Introduction

Fretting is considered as a source of wear and premature fatigue failure within mechanical parts. Fretting damage may occur whenever a junction between contacting parts is subjected to cyclic sliding micro-motions, whose characteristic amplitudes are much less than the size of the contact. Such a contact loading can be induced either by vibrations or by the application of bulk fatigue stresses to one or both of the contacting parts. The main initial damage (wear or cracking) is closely linked to the nature of the contact conditions between the contacting bodies, which depends on the contact loading, the material's bulk mechanical properties and the frictional response of the contact interface. Cracks may initiate at a very early stage and most of the component life incorporates crack growth. Due to the great need of industry to prevent fretting damage of parts rubbing against each other, like riveted joints, blade to disk fixings in jet engines, rolling bearings, a considerable attention has been devoted both experimentally and numerically. Our attention is here focused on crack initiation with the aim to predict crack behavior and propose palliatives to extend the fatigue life. Identifying the possibility of tribological fatigue at a design stage and integrate it in a predictive approach requires a multi-disciplinary phenomenological understanding which encompasses the interdependency of solid and contact mechanics, fatigue, material, wear and fretting mechanisms. The problem is further strongly multi-scale. Dimensions ranging from the meter (characteristic size of a component), to the mm (two-body contact patch between contacting components, the crack itself) down to the μm (frictional contact zone at the crack interface) are encountered. Moreover, 3D cracks located in the contact zone vicinity are submitted to multi-axial non-proportional cyclic loadings and severe stress gradients. Cracks undergo sequences of opening-closure-sticking and sliding contact conditions at interface, governing crack mixity, branching, self-arrest and propagation.

Many models and methods have been proposed to achieve the prediction of fretting crack lifetime. This involves to be able to tackle four different steps: (1) the cyclic stress–strain field computation within the safe component, accounting for the structural influence (boundary conditions, ...) but also for the contact conditions arising at the component interface; (2) the prediction of crack initiation locations and angles; (3) the crack modeling; and (4) the crack growth. The numerical simulation of each of these four steps can be achieved based on different techniques. Step 1 is easily tackled using 2D and 3D finite element techniques as long as the structural problem is relevant. Dealing with the contacting interface where the fretting cracks initiate and requiring thus accurate contact problem solution between the contacting two bodies is not so straightforward. Half-analytical and numerical techniques have been long preferred as they capture accurately and for a negligible computing effort the multi-axial stress and strain fields with severe gradients in the two-body contact vicinity. This implies to consider simplified geometries like cylinders, spheres, planes. Step 2 is concerned with multi-axial fatigue criteria either based on the concept of the critical plane like Ruiz et al. [1] or Dang Van's criterion [2] or on the concept of equivalent stress [3], strain or energy based-fracture criterion. Concerning steps 3 and 4, methods based on distributed dislocations techniques pioneered by Comninou [4], Hills and Comninou [5], Dubourg and Villechaise [6] have allowed to account for contact and frictional effects between the crack faces which govern both the crack behavior and the crack path. Dubourg and Villechaise [7] have combined this technique with a unilateral contact algorithm with friction to deal automatically with complex cyclic fretting loading conditions and multiple crack interactions. These models have been developed within the linear elastic fracture mechanics framework and 2D assumptions. They address contact fatigue problems at a local scale, dedicated to the interface between the two bodies in contact and the cracks situated in the near vicinity. Methods based on finite element techniques are able to capture the global scale of the structure (complex geometry, more realistic boundary conditions, ...) but are not accurate enough at the local scale. Further the crack growth simulation is computer time and memory demanding as it requires re-meshing and field interpolation. Large 3D crack propagation problems are thus unattainable. There is a need for robust and efficient 3D fatigue crack models accounting for frictional contact at crack interface to analyze fretting or rolling crack problems.

The extended finite element method (X-FEM) allows to deal with crack propagation without those drawbacks thanks to significant improvements in crack modeling. X-FEM is a numerical method developed within the standard finite element method framework. Its key properties are due to the partition-of-unity method developed by Melenk and Babuška [8]

combined by Moës et al. with special enriched functions added locally to the finite element approximation [9]. These enriched functions capture the asymptotic near-crack-tip behavior and the discontinuous displacement fields. Hence the initial mesh does not need to conform to the crack geometry and furthermore no re-meshing is necessary as the crack evolves during fatigue crack propagation. This method allows to deal with large 3D crack propagation problems at low computational cost and memory size. X-FEM has been applied to 3D crack growth combined with level set techniques for the crack shape description [10–13] with possible multi-scale effects [14]. The implementation within the X-FEM framework of contact with or without friction has been further performed in 2D [15–19] and in 3D [20–22]. The accurate modeling of tribological fatigue dealing with non-proportional multi-axial loading and severe stress gradients in the cracked area has been further performed [23–26]. Moreover, a methodology encompassing the cyclic contact loading determination at the interface of two components rubbing against each other, the prediction of the distribution of the crack nucleation risk at this interface and the prediction of 2D fatigue crack propagation accounting for frictional contact at the crack interface has been proposed recently within the X-FEM framework [27].

Ribeaucourt et al. [23] emphasized as an essential pre-requisite the need for a fine discretization of the crack interface to capture accurately the complex frictional contact conditions. The crack interface discretization proposed in [15] depends on the underlying finite element mesh. As a consequence, refining the crack discretization implies refining the finite element mesh. This is in conflict with the concept of crack mesh Independence inherent to X-FEM and leads to important computer time and memory cost even for two-dimensional problems. To overcome this difficulty, a two-scale X-FEM strategy was proposed in [22] to capture in a single framework the different scales involved, those of the structure, the crack and the possible localized non-linearities (confined plasticity, interfacial unilateral contact or frictional contact). The crack is considered as an autonomous entity with its own discretization scheme, variables, and constitutive law. It is connected in a weak sense to the structure and a three-mixed field formulation is used [28–30]. The interfacial discretization is further refined independently of the mesh of the structure, by successive sub-divisions of the interface elements, up to matching the scale of the contact non-linearities. This strategy has been developed and validated in a first attempt for unilateral contact at the interface of three-dimensional cracks [22].

In the present article, this model is extended to address frictional effects. Section 2 is devoted to the presentation of the X-FEM/level set numerical crack model. After recalling the definition of the global and local problems, the mixed three-field weak formulation combined with the global–local strategy is presented. The algorithm for the interface discretization refinement is described. The non-linear LATIN iterative solver is considered here. A first numerical example is performed to show the efficiency of the global–local strategy in terms of accuracy and savings in memory size. Then the combination of a non-locking LATIN and X-FEM methods (NLLA-X-FEM) is completed to avoid possible numerical oscillations when dealing with frictional contact at crack interface. A second numerical example is presented to emphasize the improvements.

Section 3 presents the application of the NLLA-XFEM model to simulate a 3D experimental fretting test with the aim of predicting fatigue life. An experimental 3D ball/plate fretting fatigue test with running conditions inducing crack nucleation and propagation is conducted. Using the actual recorded experimental fretting loading cycles, the local friction coefficient is determined. The contact pressure and traction distribution at the ball/plate interface are then computed during the fretting cycle. The crack nucleation risk distribution d is evaluated within the volume around the contact area according to Dang Van's criterion. The location and shape of the zones where the risk is the highest are in a good agreement with the two shallow cracks observed experimentally at the trailing and leading edges of the contact area. These two cracks are considered for NLLA-X-FEM simulation. The 3D crack shapes are first reconstructed from a series of metallographic observations performed on cross sections. In a second step, they are modeled using the level set technique. The sequences of contact and frictional conditions at crack interfaces are determined during the fretting cycle as well as the stress intensity factors at both crack fronts during the fretting cycle. This latter numerical simulation is performed to demonstrate the model ability to deal with challenging actual complex problems and the possibility to achieve tribological fatigue crack prediction at a design stage based on the fatigue crack modeling.

2. Global–local X-FEM model of 3D frictional contacting cracks

2.1. Three-field weak formulation of the fracture problem with frictional contact

A three-dimensional deformable cracked body $\Omega \subset R^3$ is considered with small displacement and small strain assumptions. Let $\partial\Omega$ be its boundary and $\mathbf{n}$ be the outward unit normal to $\partial\Omega$. It is submitted to imposed tractions $\mathbf{f}_t(t)$ along Γ_t and prescribed displacement $\mathbf{U}_d(t)$ along Γ_d at a given time t with a homogeneous isotropic linear elastic behavior in the bulk. Let $\mathbf{u}(t)$ be the displacement field solution, $\boldsymbol{\sigma}(t)$ the corresponding Cauchy stress tensor and $\boldsymbol{\varepsilon}(t)$ the strain tensor in the body Ω. The interface displacement field $\mathbf{w}(t)$ and the traction field $\mathbf{t}(t)$ are defined on the two crack faces Γ_C^+ and Γ_C^-. Let $\mathbf{n}_C$ and $\mathbf{t}_C$ be the outward unit normal and the tangential vectors to Γ_C^+.

The problem is partitioned in two, cf. Fig. 1. On one side, the so-called global problem referring to the structure scale, and on the other side, the so-called local problem referring to the crack scale. Both problems are defined by their own set of equations and their own primal and dual variables.

The solution of the global problem, associated to the quantities $(\mathbf{u}, \boldsymbol{\sigma})$, satisfies the equilibrium equation (1) and the constitutive law (2). It must also fulfill the mixed boundary conditions (3) and (4) along Γ_t and Γ_d.

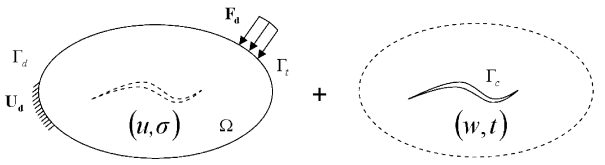

Fig. 1. The problem is divided in a global fracture problem (structure scale) and a local frictional contact problem (crack scale) with their corresponding variables and boundary conditions at a time t.

$$\text{Equilibrium} \quad \longrightarrow \quad \operatorname{div}\boldsymbol{\sigma}(t) = 0 \quad \text{in } \Omega,\ \forall t \in [0;T] \tag{1}$$

$$\text{Constitutive law} \quad \longrightarrow \quad \boldsymbol{\sigma}(t) = \mathbf{C}\boldsymbol{\varepsilon}(t) \quad \text{in } \Omega,\ \forall t \in [0;T] \tag{2}$$

$$\text{Neumann conditions} \quad \longrightarrow \quad \boldsymbol{\sigma}(t)\cdot\mathbf{n} = \mathbf{f}_t(t) \quad \text{on } \Gamma_t,\ \forall t \in [0;T] \tag{3}$$

$$\text{Dirichlet conditions} \quad \longrightarrow \quad \mathbf{u}(t) = \mathbf{U}_d(t) \quad \text{on } \Gamma_d,\ \forall t \in [0;T] \tag{4}$$

where $\mathbf{C}$ is Hooke's tensor for a homogeneous isotropic elastic material.

The quantities $(\mathbf{w},\mathbf{t})$ along Γ_C referring to the local frictional contact problem at the crack interface are expressed in the local frame $(\mathbf{n}_C,\mathbf{t}_C)$ attached to the crack as follows:

$$\mathbf{w} = \mathrm{w}_N\cdot\mathbf{n}_C + \mathrm{w}_T\cdot\mathbf{t}_C \quad \text{and} \quad \mathbf{t} = \mathrm{t}_N\cdot\mathbf{n}_C + \mathrm{t}_T\cdot\mathbf{t}_C \tag{5}$$

The opening and slip (relative displacements) between the crack faces are defined at a given time t as the evolution of the displacements between two points $G^+\in\Gamma_C^+$ and $G^-\in\Gamma_C^-$ at a given coordinate $x\in\Gamma_C$:

$$\big[\mathbf{w}_N(x,t)\big] = \mathbf{w}_N^+(x,t) - \mathbf{w}_N^-(x,t) \quad \text{and} \quad \big[\mathbf{w}_T(x,t)\big] = \mathbf{w}_T^+(x,t) - \mathbf{w}_T^-(x,t) \tag{6}$$

The solution $(\mathbf{w},\mathbf{t})$ of this local problem obeys an interfacial constitutive law between the crack faces Γ_C^+ and Γ_C^-. Coulomb's friction law is considered here:

$$\text{contact zone} \quad \big[\mathbf{w}_N(x,t)\big] = 0 \quad \Rightarrow \quad \mathbf{t}_N^+(x,t) = -\mathbf{t}_N^-(x,t) \quad \text{and} \quad \mathbf{t}_T^+(x,t) = -\mathbf{t}_T^-(x,t) \tag{7}$$

$$\text{open zone} \quad \big[\mathbf{w}_N(x,t)\big] > 0 \quad \Rightarrow \quad \mathbf{t}^+(x,t) = \mathbf{t}^-(x,t) = 0 \tag{8}$$

$$\text{stick zone} \quad \big\|\mathbf{t}_T(x,t)\big\| < \mu_C\cdot\big\|\mathbf{t}_N(x,t)\big\| \quad \Rightarrow \quad \Delta\big[\mathbf{w}_T(x,t)\big] = 0 \tag{9}$$

$$\text{slip zone} \quad \big\|\mathbf{t}_T(x,t)\big\| = \mu_C\cdot\big\|\mathbf{t}_N(x,t)\big\| \quad \Rightarrow \quad \exists\gamma>0/\Delta\big[\mathbf{w}_T(x,t)\big] = -\gamma\cdot\mathbf{t}_T^+(x,t) \tag{10}$$

where Δ corresponds to an increment of the considered quantity between two successive time steps and μ_C is the friction coefficient between the crack faces.

The link between the global and the local problems is ensured by enforcing the continuity conditions between the primal ($\mathbf{u}$ and $\mathbf{w}$) and dual fields ($\boldsymbol{\sigma}$ and $\mathbf{t}$) respectively, whose strong form is given by:

$$\mathbf{u}(t) = \mathbf{w}^+(t) \quad \text{on } \Gamma_C^+ \quad \text{and} \quad \mathbf{u}(t) = \mathbf{w}^-(t) \quad \text{on } \Gamma_C^-,\ \forall t\in[0;T] \tag{11}$$

$$\boldsymbol{\sigma}(t)\cdot\mathbf{n}_C = \mathbf{t}^+(t) \quad \text{on } \Gamma_C^+ \quad \text{and} \quad \boldsymbol{\sigma}(t)\cdot\mathbf{n}_C = \mathbf{t}^-(t) \quad \text{on } \Gamma_C^-,\ \forall t\in[0;T] \tag{12}$$

In the proposed approach, Eqs. (1), (3), (4), (11) and (12) are merged into a single three-field weak formulation:

$$\begin{aligned} 0 = &-\int_\Omega \boldsymbol{\sigma}(t):\boldsymbol{\varepsilon}(\mathbf{u}^*)\,\mathrm{d}\Omega + \int_{\Gamma_t}\mathbf{f}_t(t)\cdot\mathbf{u}^*\,\mathrm{d}S + \int_{\Gamma_C}\boldsymbol{\lambda}(t)\cdot\mathbf{u}^*\,\mathrm{d}S \\ &+ \int_{\Gamma_C}\big(\mathbf{t}(t)-\boldsymbol{\lambda}(t)\big)\cdot\mathbf{w}^*\,\mathrm{d}S \\ &+ \int_{\Gamma_C}\big(\mathbf{u}(t)-\mathbf{w}(t)\big)\cdot\boldsymbol{\lambda}^*\,\mathrm{d}S \\ &\forall\mathbf{u}^*\in U_0^*,\ \forall\mathbf{w}^*\in W^*,\ \forall\boldsymbol{\lambda}^*\in\Lambda^*,\ \forall t\in[0;T] \end{aligned} \tag{13}$$

where the global and virtual displacement fields $\mathbf{u}$ and $\mathbf{u}^*$ respectively, belong to function spaces defined by:

$$\mathbf{u}\in U, \quad U = \big\{\mathbf{u}+\text{regularity}/\mathbf{u}(t)=\mathbf{U}_d(t)\text{ on }\Gamma_d\big\} \tag{14}$$

$$\mathbf{u}^*\in U_0^*, \quad U_0^* = \big\{\mathbf{u}^*+\text{regularity}/\mathbf{u}^*=0\text{ on }\Gamma_d\big\} \tag{15}$$

From a general point of view, the displacement field **w**, traction field **t** and Lagrange multiplier field **λ** along the crack faces used in this paper are assumed to be sufficiently smooth and regular. Similar assumptions are considered for the virtual fields $\mathbf{w}^*$ and $\boldsymbol{\lambda}^*$.

It is well known that the existence and unicity of the solution of a discrete mixed formulation require a continuous definition of the Lagrange multiplier space in accordance with the displacement space, satisfying the LBB inf-sup condition. Comments and details regarding this question within X-FEM models with contact and friction can be found in [31–33,21, 34,20,19]. Additional remarks will be exposed in the next sections regarding the unilateral or frictional contact problems.

2.2. Global–local X-FEM discretization of the three-field weak formulation

The Extended Finite Element Method (X-FEM) has shown to be very efficient to model fracture problems. It is an extension of the Finite Element Method (FEM) and it is based on the partition of unity concept [8]. This method alleviates much of the burden associated with the mesh generation, by not requiring the Finite Element mesh to conform to the discontinuity. Indeed, a discontinuous function and asymptotic crack tip displacement fields are added to the FEM approximation to account for the crack. The enriched shape functions are associated to new degrees of freedom and the X-FEM displacement field approximation at a given time t is:

$$\mathbf{u}(\mathbf{x},t) \simeq \sum_{i\in N_{nodes}} \mathbf{u}_i(t)\Phi_i(\mathbf{x}) + H(\mathbf{x}) \sum_{j\in N_{crack}} \mathbf{a}_j(t)\Phi_j(\mathbf{x}) + \sum_{l=1}^{4} B_l \sum_{k\in N_{front}} \mathbf{b}_{lk}(t)\Phi_k(\mathbf{x}) \tag{16}$$

where $\mathbf{u}_i$ are the standard Finite Element degrees of freedom, $\mathbf{a}_j$ are the degrees of freedom linked to the generalized Heaviside function H and $\mathbf{b}_{lk}$ are the degrees of freedom linked to the singular enrichment functions B_l of the crack front [9,12]. Φ_i, Φ_j and Φ_k are first order shape functions. A similar approximation is used for the virtual displacement field $\mathbf{u}^*$.

The X-FEM gives a good approximation of the displacement field with coarse meshes compared to those employed when dealing with the FEM, thanks to the asymptotic crack tip enrichments [9,12]. In this paper, a standard X-FEM approach is used. However, it is not a restriction as recent improvements (treatment of blending elements or new discontinuous enrichments for instance) [18,32,31] can be easily accounted for. Furthermore, X-FEM is well adapted for modeling crack growth, as both field interpolation and re-meshing are not required during the possible crack propagation.

According to [12,13,35], a set of two three-dimensional level sets defines the crack geometry, one for the crack surface and a second one, locally orthogonal, for the crack front. This level set method also allows a robust and accurate definition of the local enrichments associated to three-dimensional cracks and greatly facilitate the update of the crack geometry during the possible propagation [12,35]. Note that discontinuous H and singular B_l enrichment functions are expressed in terms of the level set functions and the crack discontinuity is thus accurately located.

The numerical integration of the frictional contact law requires the discretization of the displacement and traction fields, **w** and **t** respectively, as well as the Lagrange multiplier field **λ**. The method proposed by Dolbow et al. in 2D [15] is extended to three-dimensional configurations: interface elements are created at the intersection of the 3D structure finite element mesh and the crack geometry. Quadrature Gauss points $G^{+/-}$ are defined on both upper (Γ^+) and lower (Γ^-) crack faces on each interface element. $\mathbf{w} = (w_x, w_y, w_z)$, $\mathbf{t} = (t_x, t_y, w_z)$ and $\boldsymbol{\lambda} = (\lambda_x, \lambda_y, \lambda_z)$ are interpolated using first order shape functions on the resulting distribution of Gauss points. Similar approximations are used for the virtual fields $\mathbf{w}^*$, $\mathbf{t}^*$ and $\boldsymbol{\lambda}^*$.

Ribeaucourt et al. [23] emphasized the need for a fine discretization of the crack interface to capture complex frictional contact conditions. This is an essential pre-requisite to accurately simulate the crack behavior. Moreover, the traction and shear distributions as well as the displacements at the crack interface are involved in the foreseen computation of the stress intensity factors and, thus, in the estimation of the propagation rate and the determination of the growth direction. The crack discretization proposed by Dolbow et al. [15] being dependent on the underlying finite element mesh, a local refinement of the finite element mesh around the crack is required to get an accurate description of the frictional contact conditions between the crack faces, cf. Fig. 2(a). This strategy conflicts with the concept of crack/mesh Independence inherent to X-FEM. Moreover, it is very laborious and CPU time consuming in 2D and prohibitive in 3D. Therefore, a different strategy was proposed by Pierres et al. [22]. It is based on the concept of Independence between the structure finite element mesh and the crack interface discretization leading to the proposed "global–local strategy". The aim is to get an accurate interfacial frictional contact solution while keeping the X-FEM benefits. This strategy is illustrated in a two-dimensional configuration in Fig. 2. It consists in increasing the number of interface elements by subdivision (h-refinement) while keeping the underlying finite element mesh unchanged. In the three-dimensional case, unequally sized and distorted interface elements may result initially from the intersection of the crack with the 3D finite element mesh. In this respect, specific shape and size indicators have been developed in order that the interface element edges cannot exceed a critical length l_C and that very acute angles are avoided. As a consequence, the successive subdivisions of 2D interface elements lead to an optimal spatial distribution of the integration Gauss points automatically adapted to the required scale. Hence, possible inaccuracy in the numerical integration is avoided.

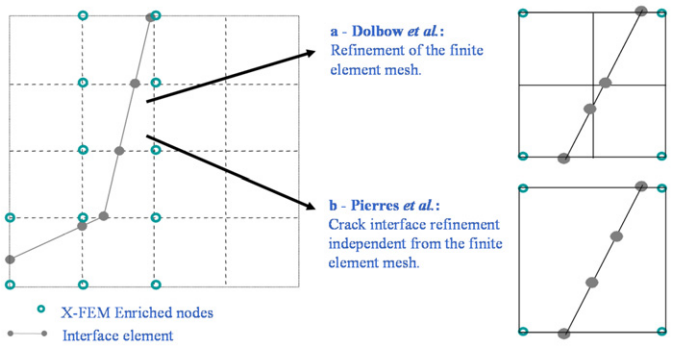

Fig. 2. Crack discretization strategies within X-FEM in the 2D case according to: (a) Dolbow et al. [15]; (b) Pierres et al. [22].

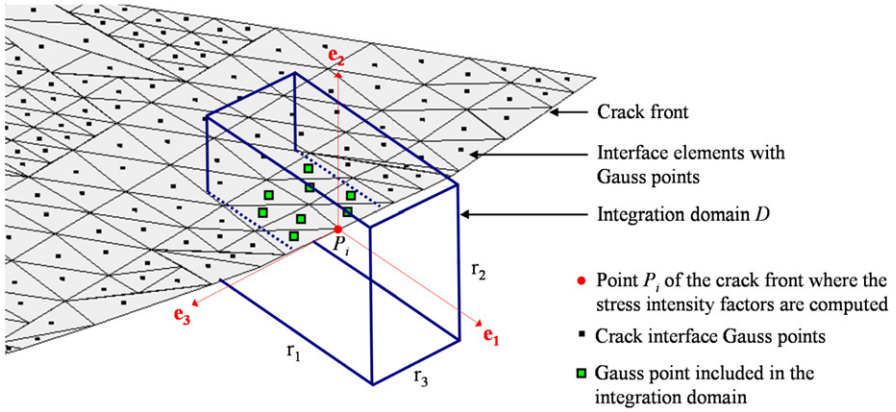

Fig. 3. Geometrical representation of the domain integral used to compute the interaction integral along the crack front with associated interface Gauss points.

2.3. Stress intensity factor calculation

The next step is concerned with the quantification of the crack severity. Fracture parameters such as the Stress Intensity Factors (SIF) or the energy release rate are measures of the intensity of the crack front fields. Specific domain integrals for extracting mixed mode SIFs along curved three-dimensional cracks derived [36–38] under the assumption of contact free faces have been implemented within the X-FEM framework [9,11]. This method has been extended to evaluate elastic T-Stress along three-dimensional cracks [39], to extract 3D SIFs dealing with confined plasticity [40] and more recently to compute mixed mode SIFs for curved bimaterial interfacial cracks in non-uniform temperature fields [41]. J and interaction integrals have been formulated for a finite element modeling of 2D frictional contact crack [15,42,23].

Following Refs. [37] and [15], an expression for the interaction integral is derived in the 3D case accounting for contact and friction along the crack faces, cf. Fig. 3:

$$I_h = -\int_D \left(\sigma_{kl}^h \epsilon_{kl}^{aux}\delta_{ij} - \sigma_{kj}^h u_{k,i}^{aux} - \sigma_{kj}^{aux} u_{k,i}^h\right) q_{i,j}\,\mathrm{d}V - \int_{\Gamma_C^+\cup\Gamma_C^-} \left(\sigma_{k2}^h u_{k,1}^{aux} + \sigma_{k2}^{aux} u_{k,1}^h\right) q_1 n_2\,\mathrm{d}S \tag{17}$$

It is worth noting that the term corresponding to contact and frictional effects along the crack front is the term including the integral over $\Gamma_C^+ \cup \Gamma_C^-$. Eq. (17) is computed over a chosen 3D domain D around discrete points P_i located along the crack front, where the virtual extension field q is assumed to be a sufficiently smooth weighting function which takes a value of unity at the crack tip and vanishes on the edge of the integral domain D [43]. h and aux correspond respectively to X-FEM numerical quantities and auxiliary fields according to asymptotic Westergaard analytical solutions for pure mode I, mode II and mode III. σ_{k2}^{aux} vanishes on Γ_C^+ and Γ_C^- as the auxiliary fields satisfy traction-free crack faces [15]. It leads to the following expression

$$I_h = -\int_D \left(\sigma_{kl}^h \epsilon_{kl}^{aux}\delta_{ij} - \sigma_{kj}^h u_{k,i}^{aux} - \sigma_{kj}^{aux} u_{k,i}^h\right) q_{i,j}\,\mathrm{d}V - \int_{\Gamma_C^+\cup\Gamma_C^-} \mathbf{t}_k^h u_{k,1}^{aux} q_1\,\mathrm{d}S \tag{18}$$

For the numerical evaluation of the above integral, the local contact traction field $\mathbf{t}$ is computed at every interface Gauss point located inside the 3D domain integral D, cf. Fig. 3. Stress intensity factors $K_{h=[1,2,3]}$ are estimated using the corresponding pure mode h analytical auxiliary fields according to:

$$K_h = \frac{E}{(1-\nu^2)} \cdot I_h \tag{19}$$

These formulas will be used hereafter to compute 3D SIFs in the different problems proposed in this article.

2.4. Unilateral contact solution

The solution of the problem defined in Section 2.1 is performed according to LArge Time INcrement method (LATIN) introduced by Ladevèze in 1985 [29] and applied to frictional contact problems by Champaney [30]. See also [44]. It was notably used in 2D X-FEM crack model with frictional contact under uniaxial static loading [15] and multi-axial quasi-static loading [23,18]. It was also employed in a 3D X-FEM crack model with unilateral contact [22].

The LATIN method consists in dividing the set of equations into two subsets, the local non-linear one and the linear global one. At a given time t, an approximate solution $s = s(\mathbf{u}, \boldsymbol{\sigma}, \mathbf{w}, \mathbf{t})$ is obtained according to an iterative process in two stages for each iteration i:

- A non-linear local step: solution $s_{i+\frac{1}{2}}$ of the local equations of the frictional contact problem at the crack interface. A local contact indicator between each couple of integration points, described in Ref. [23], allows to update the contact zones and to determine the local tangential frictional contact condition (slip or stick) according to $\mathbf{w}_i$ and $\mathbf{t}_i$ values, with respect to the frictional contact law (7), (8), (9) and (10) and to the following equation:

$$\mathbf{t}_{i+\frac{1}{2}} - \mathbf{t}_i = k_l(\mathbf{w}_{i+\frac{1}{2}} - \mathbf{w}_i) \tag{20}$$

  where k_l is a strictly positive parameter, called "local search direction", set by the user. The new interface fields $\mathbf{w}_{i+\frac{1}{2}}$ and $\mathbf{t}_{i+\frac{1}{2}}$ are computed for both normal and tangential problems.
- A global step: solution s_{i+1} of the global structure problem. Here, Eq. (21) is used in conjunction with the weak form (13), leading to (22):

$$\mathbf{t}_{i+1} - \mathbf{t}_{i+\frac{1}{2}} = -k_g(\mathbf{w}_{i+1} - \mathbf{w}_{i+\frac{1}{2}}) \tag{21}$$

$$\begin{aligned} 0 = &-\int_{\Omega} \boldsymbol{\sigma}_{i+1} : \boldsymbol{\varepsilon}(\mathbf{u}^*)\,\mathrm{d}\Omega + \int_{\Gamma^t} \mathbf{f}_t \cdot \mathbf{u}^*\,\mathrm{d}S + \int_{\Gamma_C} \boldsymbol{\lambda}_{i+1} \cdot \mathbf{u}^*\,\mathrm{d}S \\ &+ \int_{\Gamma_C} (\mathbf{t}_{i+\frac{1}{2}} + k_g \mathbf{w}_{i+\frac{1}{2}}) \cdot \mathbf{w}^*\,\mathrm{d}S - \int_{\Gamma_C} (\boldsymbol{\lambda}_{i+1} + k_g \mathbf{w}_{i+1}) \cdot \mathbf{w}^*\,\mathrm{d}S \\ &+ \int_{\Gamma_C} (\mathbf{u}_{i+1} - \mathbf{w}_{i+1}) \cdot \boldsymbol{\lambda}^*\,\mathrm{d}S \quad \forall \mathbf{u}^* \in U_0^*,\ \forall \mathbf{w}^* \in W^* \text{ and } \forall \boldsymbol{\lambda}^* \in \Lambda^* \end{aligned} \tag{22}$$

  where k_g is a strictly positive parameter set by the user, called "global search direction". It can be noticed that search directions values k_g and k_l only influence the convergence rate of the numerical scheme and that the method always converges toward the exact solution of the discretized problem [30]. In practice, a quasi optimal value $k_0 = k_g = k_l$ is obtained based on a material property (Young's modulus for instance) and a characteristic length (in 2D) or area (in 3D) linked to the crack [30,29,22].

Introducing the enriched displacement field (16) and the discretized quantities on the crack faces in Eq. (22) yields the linear system (23):

$$\begin{bmatrix} \mathbf{K}_{uu} & 0 & -\mathbf{K}_{u\lambda} \\ 0 & \mathbf{K}_{ww} & \mathbf{K}_{w\lambda} \\ -\mathbf{K}_{u\lambda}^T & \mathbf{K}_{w\lambda}^T & 0 \end{bmatrix} \begin{pmatrix} \mathbf{U}_{i+1} \\ \mathbf{W}_{i+1} \\ \boldsymbol{\Lambda}_{i+1} \end{pmatrix} = \begin{pmatrix} \mathbf{F}_t \\ \mathbf{K}_{w\lambda} \cdot \mathbf{T}_{i+\frac{1}{2}} + \mathbf{K}_{ww} \cdot \mathbf{W}_{i+\frac{1}{2}} \\ 0 \end{pmatrix} \tag{23}$$

where $\mathbf{K}_{uu}$ is the stiffness matrix of the structure. The "mortar" operators $\mathbf{K}_{u\lambda}^T$ and $\mathbf{K}_{w\lambda}^T$ ensure the weak link between the local and global problems and enable the use of incompatible discretizations between the crack interface and the structure. $\mathbf{K}_{ww}$ is the operator associated to the global search direction k_g.

The linear system (23) being solved, the local traction $\mathbf{T}_{i+1}$ is computed according to (21). The local and the global steps are repeated until the convergence is achieved. according to a specific local convergence criterion developed by Ribeaucourt

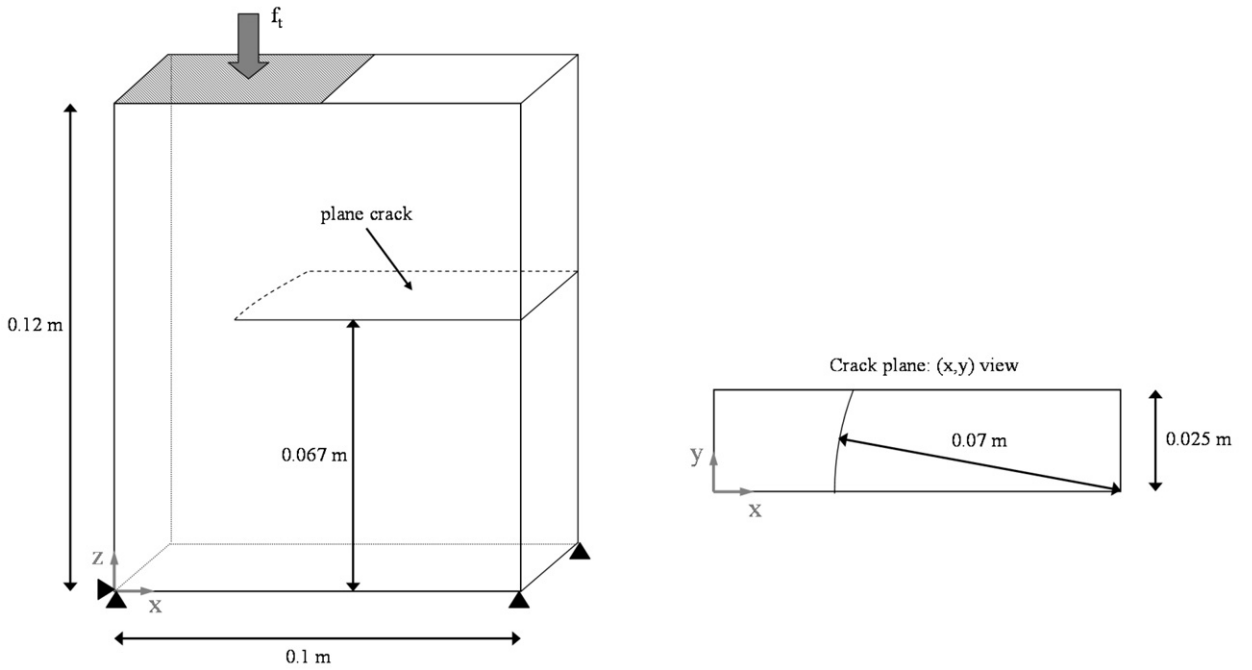

Fig. 4. Problem 1: cracked domain with boundary and loading conditions; (X, Y) view of the crack plane at $z = 0.07$ m.

et al. [23]. It is defined as the distance between the global and the local approximations, referring to both interface displacements and loads for the normal and tangential problems. Remark: When convergence is achieved, $\boldsymbol{\Lambda} = \mathbf{T}$ at the prescribed accuracy.

The proposed 3D X-FEM crack model devoted to unilateral frictional contact solution on the crack interface rests on an original global–local strategy. The following Problem 1 is used here to demonstrate the ability of the model to accurately capture complex discontinuous contact conditions holding at a scale lower than the scale of the finite element mesh, in other words when the stick-slip transition or open-closed transition occurs inside a finite element.

Problem 1. A 3D (0.1 m × 0.025 m × 0.12 m) parallelepipedic specimen with a surface breaking plane crack with a curved front is considered. The detailed geometry of the cracked sample is depicted in Fig. 4. Young's modulus and Poisson's ratio are respectively $E = 206$ GPa, $\nu = 0.3$. Dirichlet boundary conditions $u_Z = 0$ are imposed on the bottom surface and rigid body displacements are blocked. A compressive uniform loading $f_t = 100$ MPa is applied on half of the top surface to induce both contacting and open areas along the crack interface. A unilateral contact law without friction is considered between the crack faces. Three configurations labeled 1, 2 and 3 are considered:

- 1: A rather fine structure finite element mesh is used (104 544 tetrahedra). The ratio between the characteristic length of the crack and the characteristic length of the 3D finite elements in the zone of interest is $R = 14$. The crack interface discretization is defined according to the method proposed by Dolbow et al. [15]. No refinement is used, leading to a distribution of 2049 interface Gauss points. Case 1 is considered as the reference case.
- 2: A rather coarse structure finite element mesh is used (3456 elements, $R = 5.5$). The crack interface discretization is defined according to [15] again, leading to a distribution of 260 interface Gauss points.
- 3: The structure finite element mesh of case 2 is used again (3456 elements, $R = 5.5$). The proposed global–local strategy is achieved. The crack discretization refinement is performed considering a critical size for the interface element edges equal to $l_c = 1.8$ mm, leading to a 2076 Gauss point distribution at the crack interface.

For each case, the optimal convergence rate is obtained using a single value for the two search directions $k_0 = k_l = k_g = 10^{+13}$ Pa m^{-1}. The approximation of the contact solution is performed at a given accuracy of 10^{-3} according to the local convergence criterion developed in [23]. Fig. 5 shows the structure finite element mesh, the crack interface discretization and the computed local traction field $\mathbf{T}$ in the area of interest for each case.

According to the reference case 1, combined fine finite element mesh and fine crack interface discretization give accurate results and capture precisely the transition between the open ($\mathbf{T} = 0$) and closed ($\mathbf{T} > 0$) areas along the crack faces, located at $x = 19$ mm. Nevertheless, the use of a locally refined finite element mesh in the vicinity of the crack requires important numerical efforts and conflicts with the mesh Independence concept inherent to X-FEM.

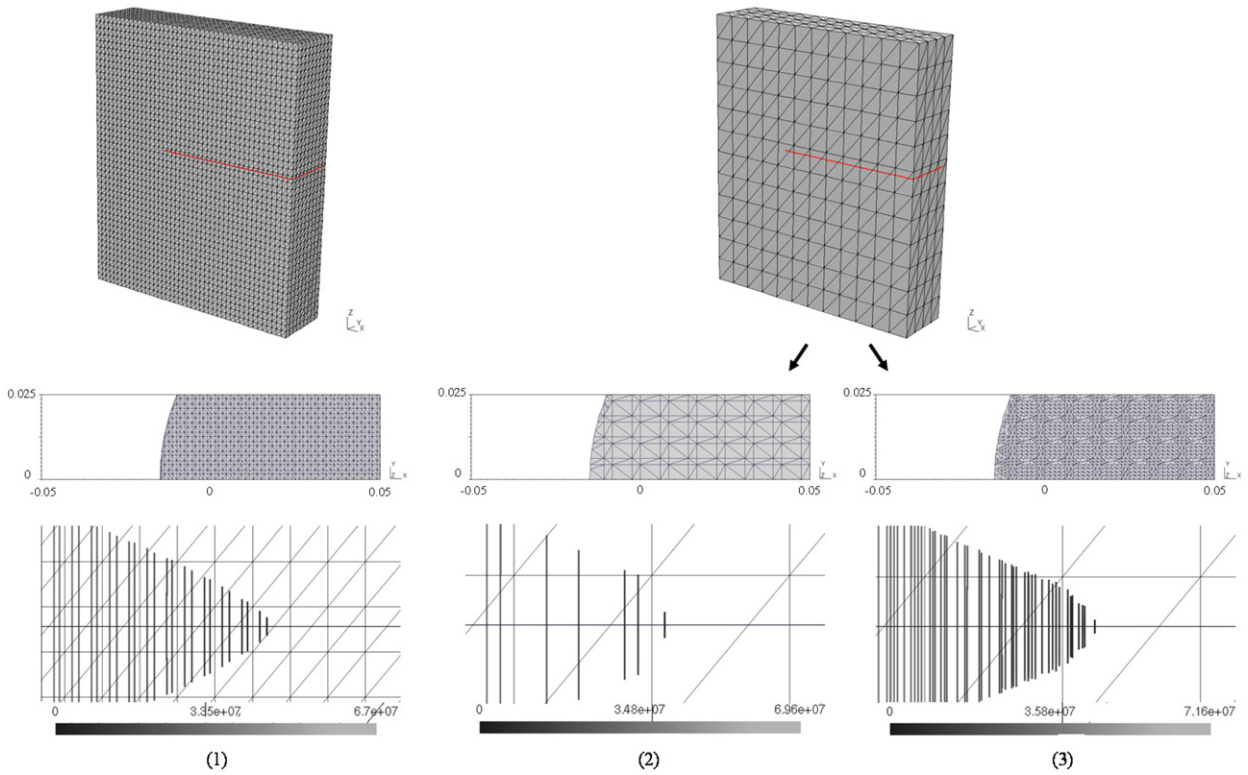

Fig. 5. Fine and coarse meshes of the structure, discretizations of the crack interface with triangular interface elements, and (x, z) views of the computed traction field in Pa along the crack interface represented with lines according to cases (1), (2), and (3).

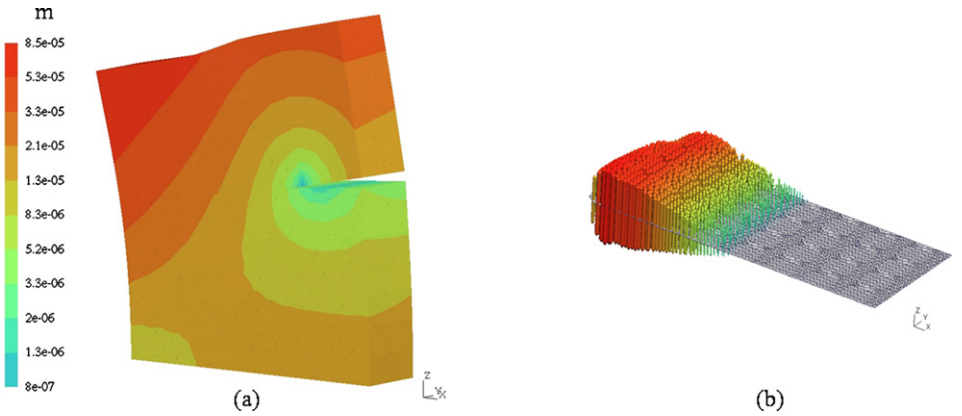

Fig. 6. (a) Amplified representation of the global displacement field in m ($\times 200$); (b) Three-dimensional representation of the traction field along the crack interface (case 3).

In case 2, coarse finite element mesh and coarse crack interface discretization do not allow a fine description of the local unilateral contact conditions. **t** and **w** variations are approximated roughly and the boundary between the open and closed areas is not accurately captured: $x = 17.3$ mm.

In case 3, the computed local solution is very close to the one obtained according to the reference case 1. The contact solution is accurately captured using a refined crack interface discretization adapted to the scale of the local problem, independently from the finite element mesh in the bulk. The location of the discontinuity between the open and contacting areas is quantified accurately at $x = 18.7$ mm. The CPU time is further significantly reduced with a save-up of 75% with respect to the reference case 1. An other key issue is that no numerical oscillation of the computed primal and dual interface variables **W** and **T** along the crack faces is observed although a consequent refinement of the Lagrangian multiplier space is conducted, cf. Fig. 6. This result confirms the good properties of the mixed three-field weak formulation and shows the ability of the proposed model to capture complex local unilateral contact conditions at a lower scale than the characteristic

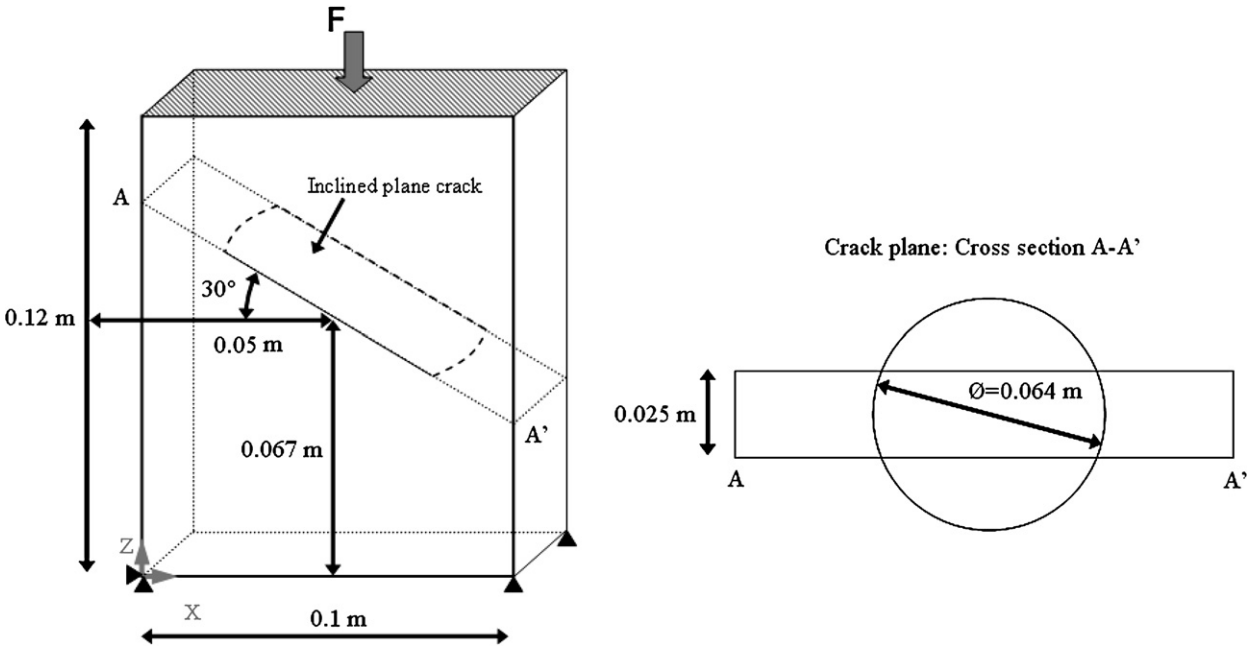

Fig. 7. Problem 2: cracked domain with boundary and loading conditions; Crack geometry in cross section A-A′.

one of the finite element structure mesh [22]. Note that the stress intensity factor K_I is not computed as the crack front is closed.

2.5. Non-locking frictional contact solution

However, when tangential slip occurs between the crack faces, the model shows some limitations. Indeed, numerical oscillations can be observed in the local frictional contact solution, restraining the convergence of the proposed method. Numerical experiments clearly show that the choice of the normal and tangential Lagrange multiplier space influences the stability of the three-field weak formulation. It is proposed here to improve the three-field weak formulation (13) by introducing a penalty term on the Dirichlet boundary condition between the global and local problems. Eq. (23) becomes:

$$\begin{bmatrix} \mathbf{K}_{uu} & 0 & -\mathbf{K}_{u\lambda} \\ 0 & \mathbf{K}_{ww} & \mathbf{K}_{w\lambda} \\ -\mathbf{K}_{u\lambda}^T & \mathbf{K}_{w\lambda}^T & \mathbf{A}_{\lambda\lambda} \end{bmatrix} \begin{pmatrix} \mathbf{U}_{i+1} \\ \mathbf{W}_{i+1} \\ \boldsymbol{\Lambda}_{i+1} \end{pmatrix} = \begin{pmatrix} \mathbf{F}_t \\ \mathbf{K}_{w\lambda} \cdot \mathbf{T}_{i+\frac{1}{2}} + \mathbf{K}_{ww} \cdot \mathbf{W}_{i+\frac{1}{2}} \\ \mathbf{A}_{\lambda\lambda} \cdot \boldsymbol{\Lambda}_i \end{pmatrix} \tag{24}$$

where $\mathbf{A}_{\lambda\lambda} = \alpha \cdot \mathbf{I}_d$ is the penalty operator and α is set by the user. This additional term only influences the convergence rate of the iterative scheme but does not affect the problem solution. Indeed, when convergence is achieved, $\mathbf{A}_{\lambda\lambda} \cdot \boldsymbol{\Lambda}_{i+1} - \mathbf{A}_{\lambda\lambda} \cdot \boldsymbol{\Lambda}_i = 0$ at a prescribed accuracy. Numerical experiments seem to show that the effect of this penalty term is similar to Nitsche-type approach [32,33]. Furthermore, this is very close to a Robin-type condition between the crack faces within the X-FEM framework. Numerical studies are in progress to obtain the general properties of such penalty term on the stability of the three-field weak form.

In the following Problem 2, the ability of the so-called Non-Locking LATIN Method (NLLA-X-FEM) to accurately solve frictional contacting crack problems with possible tangential sliding is demonstrated and it is shown that spurious oscillations are avoided.

Problem 2. A 3D (0.1 m × 0.025 m × 0.12 m) parallelepipedic specimen identical to the one defined in Problem 1 with a 30° inclined crack with curved fronts is considered, cf. Fig. 7. Young's modulus and Poisson's ratio are respectively $E = 206$ GPa, $\nu = 0.3$. Dirichlet boundary conditions $u_Z = 0$ are imposed on the bottom surface and rigid body displacements are blocked. A compressive uniform loading $f_t = 100$ MPa is applied on the top surface.

The frictional Coulomb's law expressed by (7), (8), (9) and (10) is considered. A rather coarse structure finite element mesh (3456 tetrahedra) is defined. The crack interface discretization is refined according to the global–local strategy proposed in this paper. The critical size chosen for the interface element edges is $l_C = 1.8$ mm. A distribution of 1670 interface Gauss points is obtained, cf. Fig. 8. The approximation of the solution is computed with a given accuracy of 10^{-4}, using both the Standard LATIN X-FEM Method (SLA-X-FEM) and the proposed Non-Locking LATIN X-FEM Method (NLLA-X-FEM) to illustrate the improvements and the stability of this latter method. The optimal convergence rate is obtained using a single

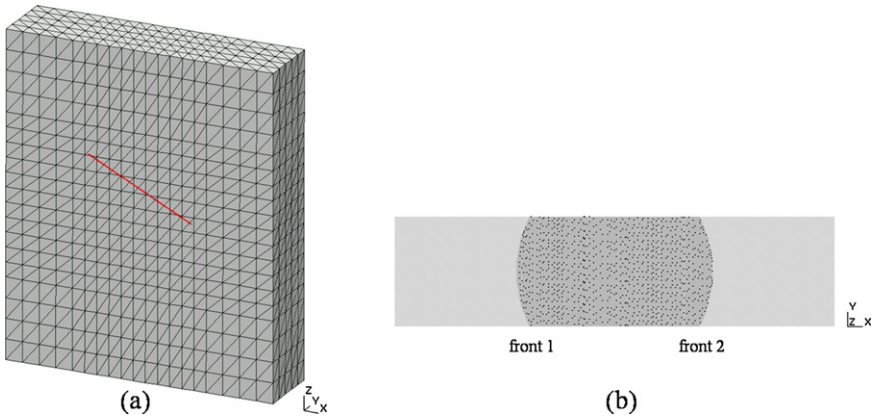

Fig. 8. 3D structure mesh and refined crack interface discretization.

value for the two search directions $k_0 = k_l = k_g = 10^{+13}$ Pa m^{-1} for both methods. According to the proposed NLLA-X-FEM, the best results regarding the quality of the frictional contact solution (no oscillation) and the convergence rate are obtained using a penalty term value $\alpha = -10^{-11}$ m Pa^{-1}.

Three different values of the interfacial friction coefficient are considered $\mu_C = 1$; 0.5; or 0, giving rise to different interfacial contact states: stick, partial slip, or gross slip. Illustrations of the interfacial traction field **T** and the relative tangential displacement field $[\mathbf{W}_T] = (\mathbf{W}_T^+ - \mathbf{W}_T^-)$ are given for each μ_C value according to both methods in Figs. 9, 10 and 11.

In the case of full stick or partial slip between the crack faces, i.e. $\mu_C = 1$ or 0.5, traction fields **T** computed according to SLA-X-FEM or NLLA-X-FEM are similar. The local frictional contact solutions do not show manifest numerical oscillations. Nevertheless, the SLA-X-FEM solution is notably perturbed in the crack front vicinity whereas the NLLA-X-FEM solution is smooth. Moreover, **w** solution for $\mu_C = 0.5$ is accurately captured according to the NLLA-X-FEM whereas the SLA-X-FEM does not allow a precise location of the slip and stick areas at the crack interface at a prescribed accuracy, cf. Figs. 10(a) and 10(b). Furthermore, the CPU time is significantly reduced with a save-up of 70% when using the NLLA-X-FEM, cf. Table 1.

In the case of gross slip contact at the crack interface, i.e. $\mu_C = 0$, significant oscillations perturb the SLA-X-FEM solution. See the local traction field **T** in Fig. 11(a). Furthermore, these spurious oscillations produce anomalous stress peaks along the crack interface, introducing local errors in the global solution of the problem and restraining the method convergence. However, smooth local fields are obtained according to the proposed NLLA-X-FEM and the frictional contact solution is accurately captured, cf. Figs. 10(b) and 11(b). The global solution of the problem is not perturbed and the convergence rate of the model is highly increased, cf. Table 1. Furthermore, it can be noticed that the number of iterations is independent of the value of the friction coefficient. Fig. 12 shows the convergence curves of both iterative methods. It can be noticed that the SLA-X-FEM almost stops converging at a certain point whereas the new NLLA-X-FEM proposed in this paper does not.

Remark. One can notice some local errors in the contact solution near the front. These are not related to the previously described numerical oscillations but result from the X-FEM specific enrichments near the crack tip. Recall that a standard X-FEM approach is used here. However, it can easily be extended to recent improvements (treatment of blending elements or new discontinuous enrichments for instance) [45,18,32,31].

The proposed NLLA-X-FEM model accurately captures the fine and complex solution of the frictional contact problem between crack faces at a prescribed accuracy, thanks to the independent crack interface discretization adapted to the required scale. Unstability problems (numerical oscillations) are avoided whatever the interfacial frictional contact conditions are, i.e. partial opening with stick contact, or partial slip contact, or gross slip contact, by the use of an additional penalty term on the continuity conditions connecting the global and local displacement fields **u** and **w**. Note that the quality of this contact solution is a key issue as it is involved in the computation of the stress intensity factors as described in Section 2.3, cf. Fig. 13. The influence of the friction coefficient is clearly emphasized. A stick zone extends from the crack fronts up to an interior region whose size depends on μ_C. For $\mu_C = 0.5$; and 1, the size of this region is quite large, the relative tangential displacement of the crack faces is low and similar K_{II} values are obtained. For $\mu_C = 0$, the stick region tends to disappear and K_{II} values are quite high compared to the previous ones. Note that K_{III} values are small compared to K_{II} ones and that K_I is nil whatever μ_C value.

The previous example illustrates the robustness and the efficiency of the combined NLLA-X-FEM model for 3D frictional contacting cracks based on an innovative three-field weak formulation. In the following section, the proposed NLLA-X-FEM strategy is used to model an experimental fretting fatigue crack problem.

Table 1
Number of iterations required to achieve convergence for each case and relative required CPU time according to both LATIN based methods.

Friction coefficient μ_C	1	0.5	0
SLA-X-FEM	294	286	150
NLLA-X-FEM	87	86	86
CPU time save-up	70%	70%	43%

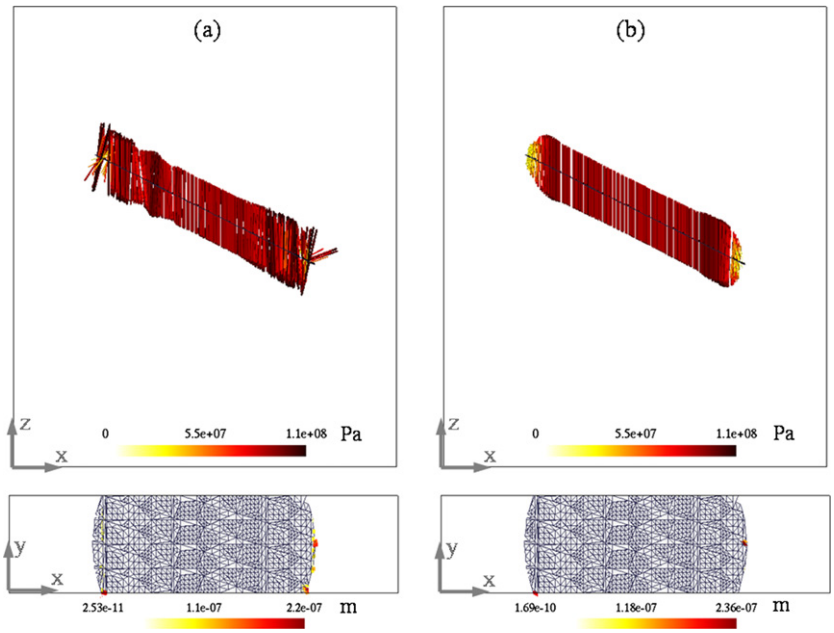

Fig. 9. $\mu_C = 1$: (X, Z) view of the local traction field $\mathbf{T}$ and (X, Y) view of the relative tangential displacements field $[\mathbf{W}_T]$. (a) SLA-X-FEM; (b) NLLA-X-FEM.

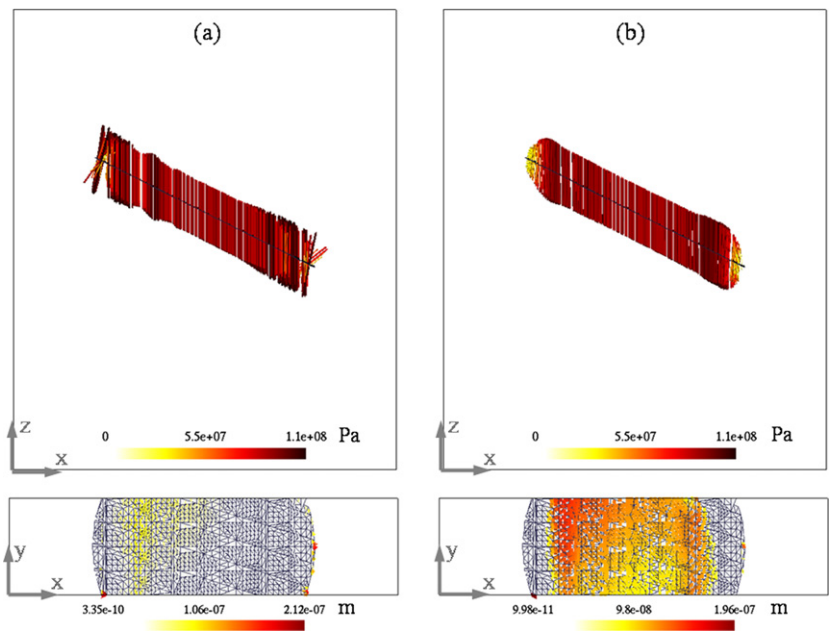

Fig. 10. $\mu_C = 0.5$: (X, Z) view of the local traction field $\mathbf{T}$ and (X, Y) view of the relative tangential displacements field $[\mathbf{W}_T]$. (a) SLA-X-FEM; (b) NLLA-X-FEM.

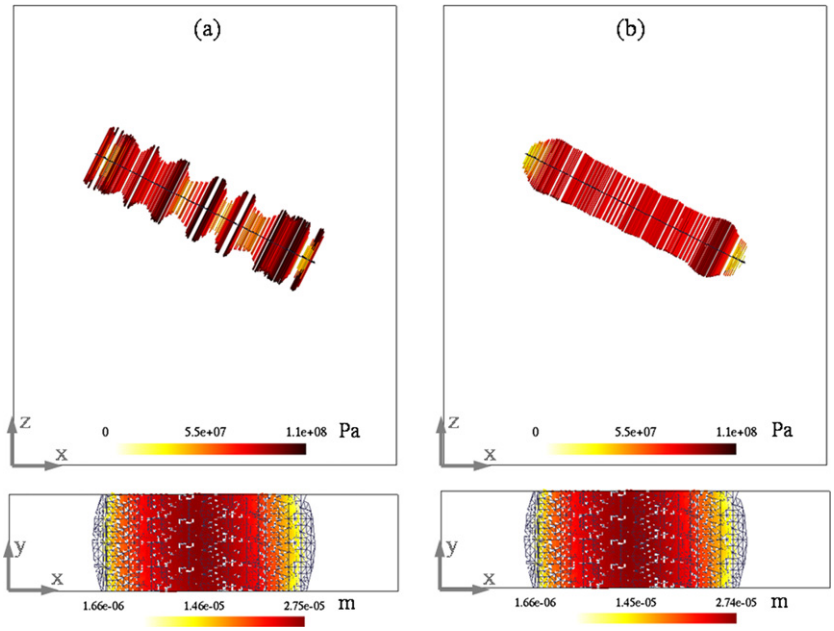

Fig. 11. $\mu_C = 0$: (X, Z) view of the local traction field $\mathbf{T}$ and (X, Y) view of the relative tangential displacements field $[\mathbf{W}_T]$. (a) SLA-X-FEM; (b) NLLA-X-FEM.

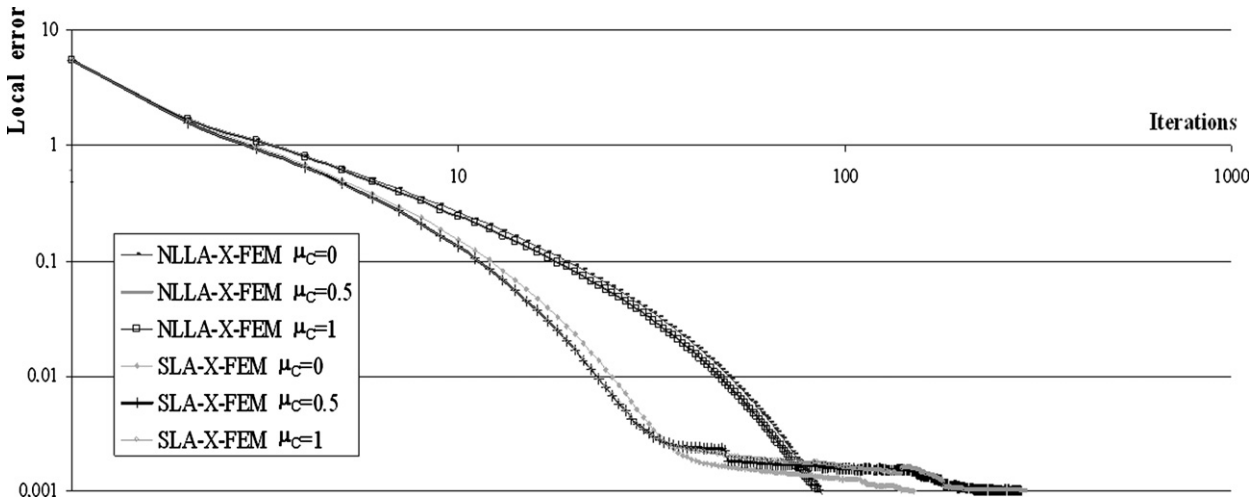

Fig. 12. Value of the local convergence criterion with respect to the iteration index for each case $\mu_C = 0$; 0.5; or 1 and for both LATIN based methods.

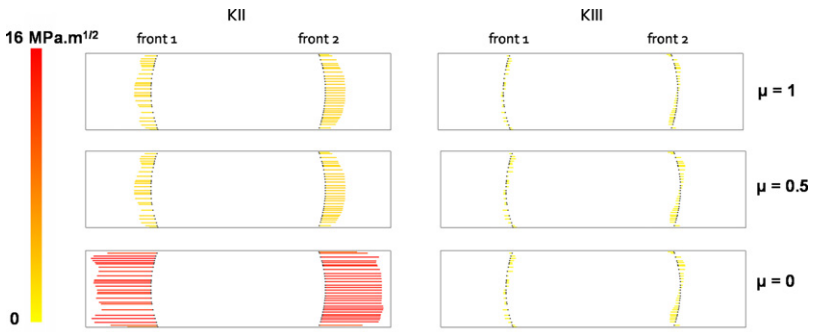

Fig. 13. Mode II and mode III stress intensity factors at both crack fronts for each μ_C value.

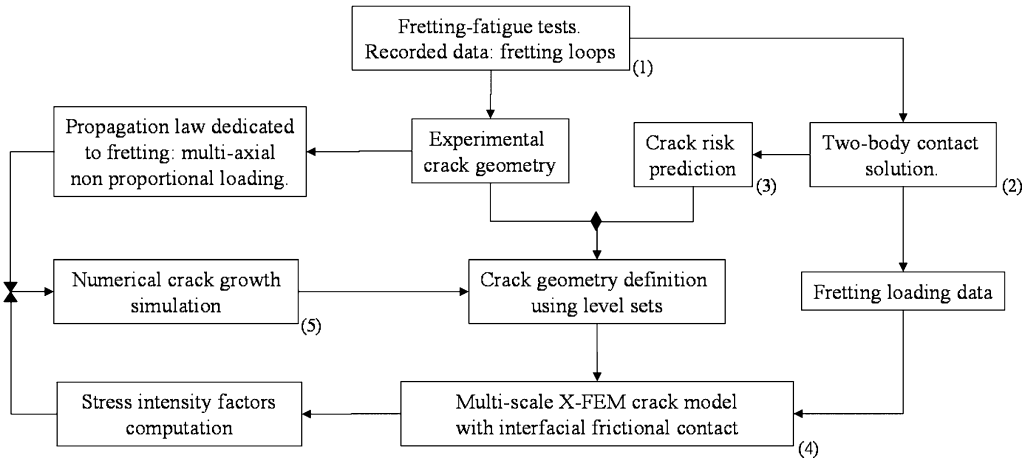

Fig. 14. Flowchart of the methodology employed here.

3. Numerical application: 3D experimental fretting-fatigue test modeling

A considerable attention has been devoted both experimentally and numerically to identify the possibility of tribological fatigue at a design stage, to integrate it in a predictive approach based on fatigue crack modeling and to propose palliatives to extend the fatigue life. An analysis of an actual experimental test is presented here. It combines experimental and numerical results. The 3D fatigue crack model based on NLLA-X-FEM approach is used here for 3D fretting crack modeling. Fretting damage may occur whenever a junction between contacting parts is subjected to cyclic sliding micro-motions, whose characteristic amplitudes are much less than the size of the contact. Such a contact loading can be induced either by vibrations or by the application of bulk fatigue stresses to one or both of the contacting parts. Various forms of damage can be observed under those conditions, such as wear and/or crack nucleation. Significant efforts have been made to acquire a better insight into fretting through a methodology combining experiments and modeling. Material Response (MRFM) and Running conditions (RCFM) Fretting Maps [46,47] have been introduced to classify through an experimental method, the type of damage (no damage, crack, wear) predominantly encountered depending on the running conditions. Those running conditions record the evolution against time of the fretting conditions (stick, partial slip or gross slip) characterized by friction loops showing the tangential force (Q) versus the contact relative displacement (δ) during a complete fretting cycle. Crack nucleation is the dominant degradation response under very small displacement amplitude at two-body interface, associated to both partial slip regime and mixed fretting regime. It is further observed at a very early stage and most of the component life incorporates crack growth. Those 3D cracks are located in the contact zone vicinity and are submitted to multi-axial non-proportional cyclic loadings and severe stress gradients. They undergo complex sequences of opening-closure-sticking and sliding contact conditions at interface, governing crack mixity, branching, self-arrest and propagation [3].

The fretting problem analysis presented here combines experimental and numerical results. Fretting tests have been carried out and the corresponding modeling has been performed. In this example, normal load-displacement pairings leading to partial slip regime have been selected. Cracking is thus the main degradation response. The methodology employed here involves five different steps summarized in the flowchart of Fig. 14: (1) fretting tests are conducted, data are recorded and analyzed, including the 3D crack geometry reconstruction from observations (2) the contact conditions at the two-body interface are computed during the fretting cycle, (3) the prediction of the crack nucleation risk according to Dang Van's criterion is performed, (4) two elliptical fretting cracks, defined from the observations performed at step 1, are modeled within X-FEM/level set framework, (5) the crack growth is achieved. Points (2) to (5) defining this methodology have been detailed in [27] in 2D. Points (1) to (4) are performed in 3D in this paper.

Step 1: Fretting experiments. An experimental fretting test is thus considered. Experimental data have been recorded continuously during the tests with careful monitoring of the displacement amplitude between the specimens, recording of the frictional forces versus the cycles. The upper body is a standard steel ball bearing with a 6.4 mm radius. The lower body is a thick steel plate (25 mm $\times$ 16 mm $\times$ 4 mm). The mechanical properties of the samples are stated in Table 2. The fretting test rig used to perform the test allows applying a controlled normal force P and a sinusoidal tangential displacement parallel to x-axis of amplitude δ on the ball at a frequency F of 20 Hz. The resulting tangential force Q is monitored. Performing measurements gives the ratio between the tangential and normal loads $f = Q/P$ that is equal to the friction coefficient μ in case of gross sliding but differs from it as soon as sticking occurs. The tests are therefore characterized by (Q–δ) curves along with the evolution of f. The loading conditions given in Table 2 have been selected so that partial slip regime is obtained throughout the test. Fig. 15(a) displays a photography of a typical fretting scar, with the circular contact area made of a central stick zone and an annulus sliding zone. Two main elliptical cracks are initiated symmetrically at both contact area edges at a very early stage in the fatigue life and have governed the component lifetime. At the end of the fretting test,

Table 2
Steel mechanical properties and fretting test loading parameters.

E	ν	P	Q	F	δ
210 GPa	0.3	120 N	95 N	20 Hz	9 μm

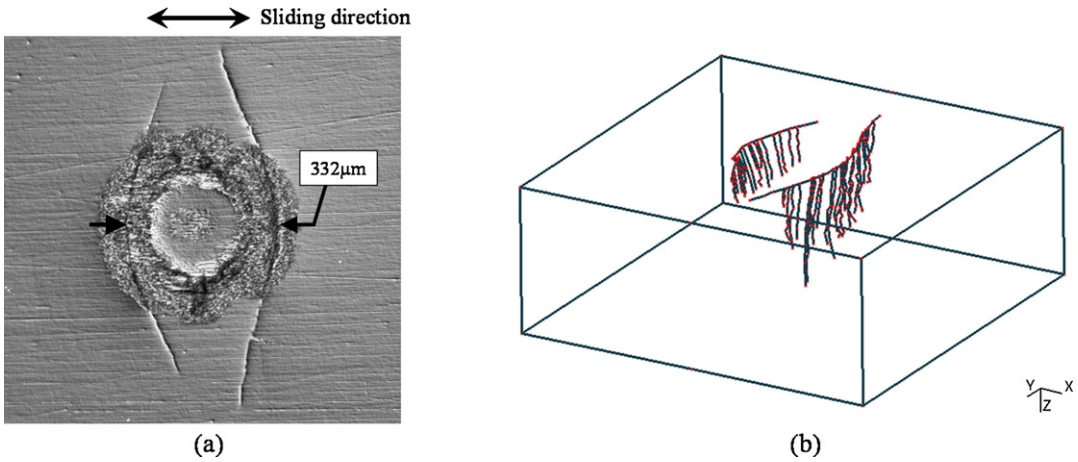

Fig. 15. (a) Microscopic view of the cracked sample surface after 50 000 fretting cycles; (b) 3D re-construction of the experimental fretting-fatigue cracks using micro-metallographic cross sections of the cracked sample.

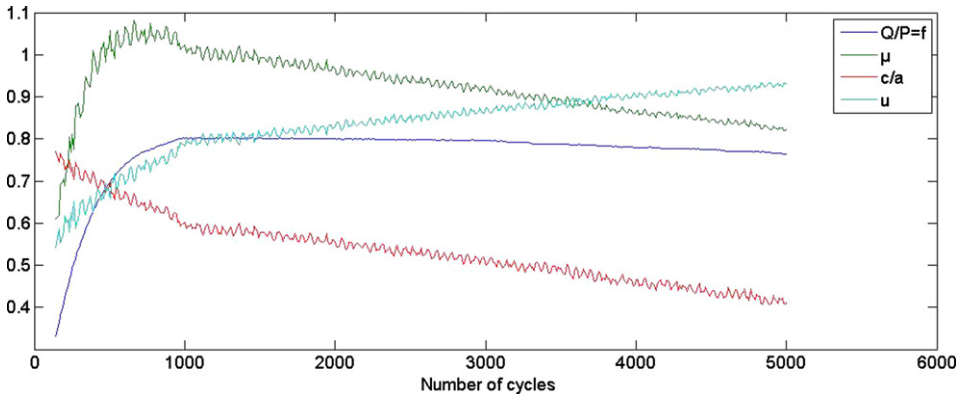

Fig. 16. Experimental evolution of f ratio versus the number of fretting cycles under partial slip regime. Determination of μ, c/a and u.

the specimen was removed and sectioned for metallographic observations. Cross-sections have been performed at different y values. 3D crack shapes have been reconstructed from the micro-metallographic analysis as seen in Fig. 15(b).

Those data coming from the experiments are used in step 4 as input data for the 3D fretting crack modeling within the X-FEM framework.

Step 2: Two-body contact solution and fretting cycle. The $(Q-\delta)$ fretting loops along with the evolution of f are used to determine the actual value of the coefficient of friction μ (see Fig. 16). The application of an energy based sliding criterion developed by Fouvry et al. [48] based on the quantification of the dissipated energy E_d corresponding to the interfacial shear work defined by the area of $(Q-\delta)$ hysteresis loop as illustrated in Fig. 17(a) combined with Mindlin's approach [49] enables one to deduce from the f ratio the actual friction coefficient μ acting in the sliding annulus using Eqs. (25) and (26):

$$A = \frac{6}{5} \cdot \frac{(1+(1-u)^{5/3}) - \frac{5}{6}u(1+(1-u)^{2/3})}{u(1+(1-u)^{2/3})} \tag{25}$$

$$u = \frac{Q^*}{\mu P} = \frac{f}{\mu} \tag{26}$$

where A is the sliding energy ratio. Since the fretting loop is recorded against time, A is computed by integrating the loop. Solving Eq. (25) yields u and finally μ is deduced. It is here equal to 0.92. Further, the comparison of the fretting loops

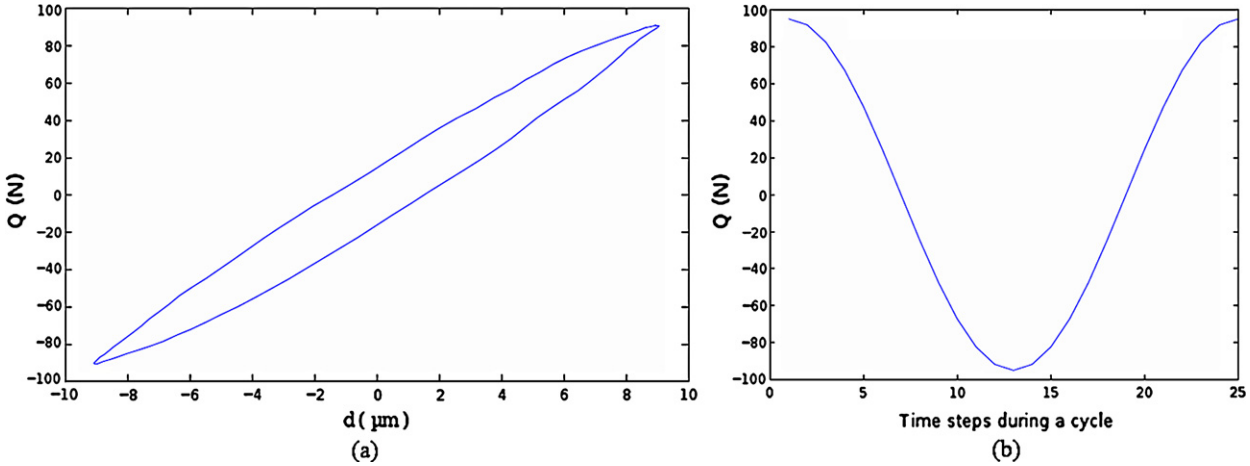

Fig. 17. Stabilized experimental fretting loop ($Q-\delta$) and Q evolution versus the time steps.

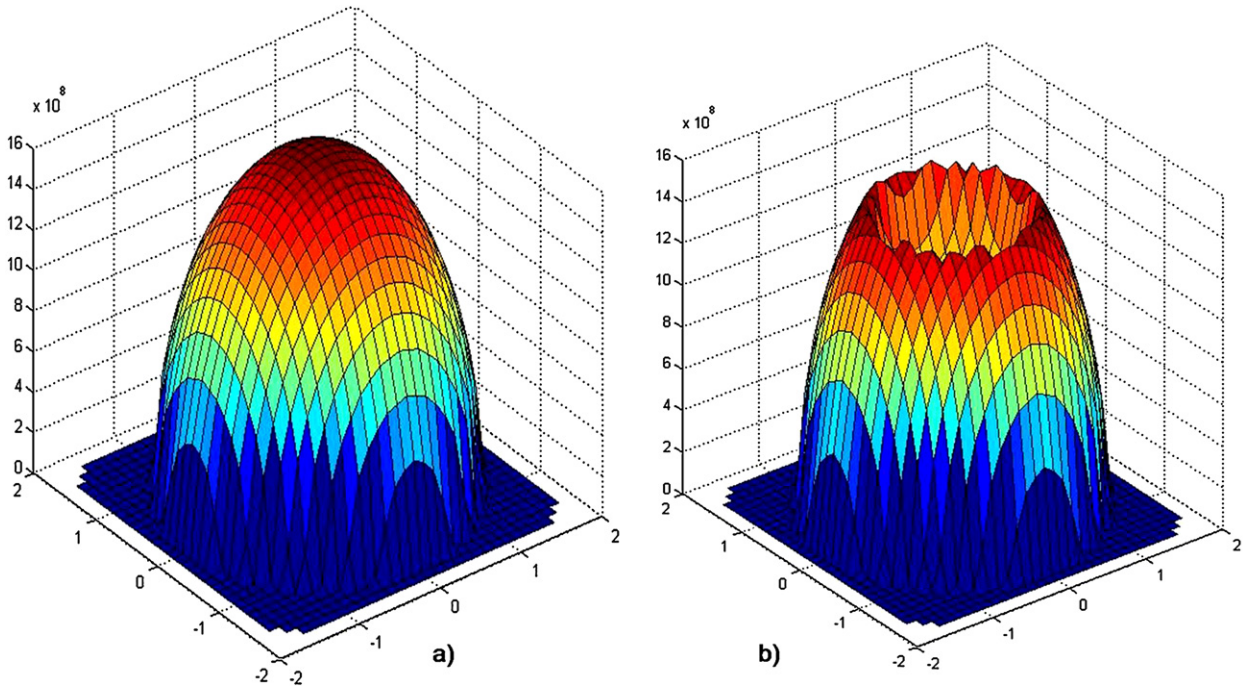

Fig. 18. (a) Pressure $p(x, y)$ and (b) traction $q(x, y, t)$ distributions for $t = 1$.

obtained by the present model based on Mindlin's solution with the experimental one provides a satisfactory agreement [50].

The pressure distribution $p(x, y)$ is then analytically computed according to Hertz's theory, cf. Fig. 18(a). The radius of the contact area a, the maximum pressure P_0 and the stick-slip ratio $k = c/a$ are equal to 171 µm, 2.05 GPa and 0.52 respectively. A sinusoidal evolution of tangential force is considered in agreement with the experiment and 25 time steps are considered to describe the fretting cycle, cf. Fig. 17(b). The resulting global traction distribution $q(x, y)$ within the contact area is obtained during the fretting cycle following Cattaneo's technique described in [51], cf. Fig. 18(b).

Step 3: Prediction of the crack nucleation risk. In order to assess the fatigue strength of the material submitted to a cyclic fretting loading, Dang Van's stress based criterion [2] has been chosen since it allows the determination of a time loading path, for t varying over a cycle, imposed on a local volume which supports multi-axial fatigue. The critical damage accumulation is based on a combination of the shear stress $\tau(t)$ acting on the plane of normal **n** along with the hydrostatic stress $\sigma_H(t)$. The characteristic relationship of this critical plane approach is then:

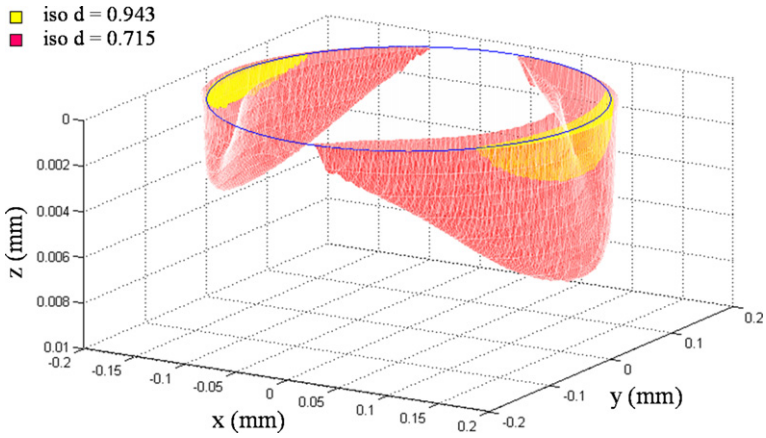

Fig. 19. Distribution of Dang Van's crack nucleation risk d computed in volume in the vicinity of the two-body contact surface.

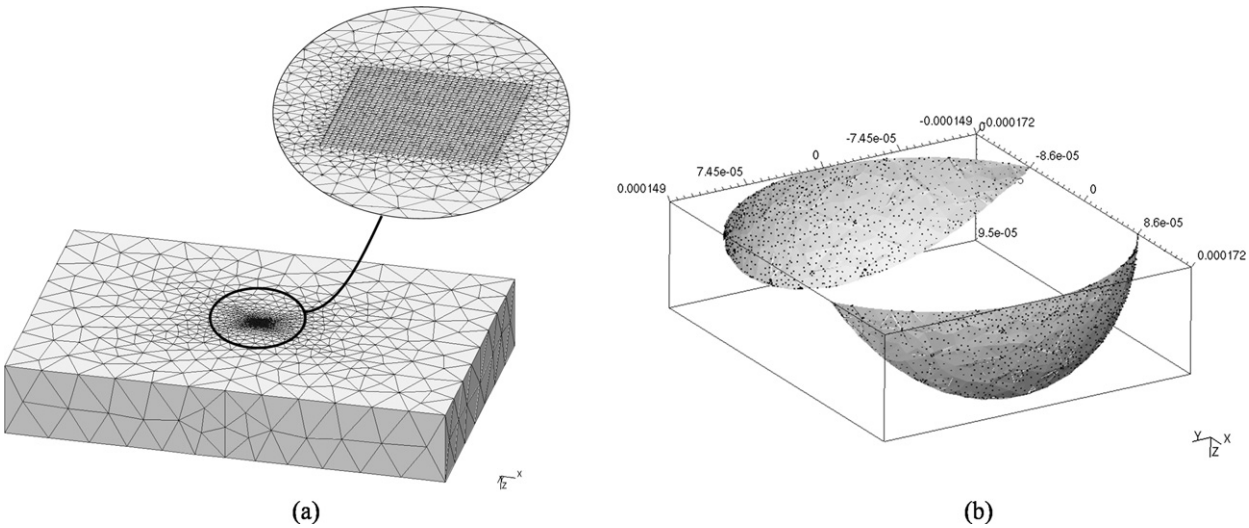

Fig. 20. (a) Mesh of the sample plate (46 266 tetrahedra); (b) Level set surfaces defining the cracks and refined crack interface discretization (1804 interface Gauss points).

$$\max_{(n)}\Big(\max_{(t)}\big(\tau(\mathbf{n},t)+\alpha\sigma_H(t)\big)\Big)=\beta \tag{27}$$

where α and β are:

$$\alpha=\frac{6t_{-1}-3f_{-1}}{f_{-1}}\qquad \beta=2t_{-1} \tag{28}$$

and f_{-1} and t_{-1} being the plain fatigue and torsion fatigue limits for a R ratio equal to -1. To observe the fatigue resistance, the couple (τ,σ_H) needs to be calculated during the loading cycle on each point for each plane direction, defined by its normal $\mathbf{n}$ and orientation θ. This process is very long and laborious and has been simplified [2] assuming Tresca's law (29) is valid.

$$\max_{(n)}\big(\tau(\mathbf{n},t)\big)=Tresca(t) \tag{29}$$

$$\mathrm{d}=\max_{(t)}\left(\frac{\sup_{(i,j)}\left(\frac{\sigma_i(t)-\sigma_j(t)}{2}\right)}{\beta-\alpha\sigma_H(t)}\right) \tag{30}$$

where σ_i and σ_j are the principal stresses. This criterion has been already applied successfully to predict the distribution of fretting crack nucleation risk. The reader is referred to [52] for further details.

The distribution of the crack nucleation risk d is here computed within the volume around the contact area and presented Fig. 19. This crack nucleation risk is close to unity in two zones, located at the border of the contact zone and whose shapes

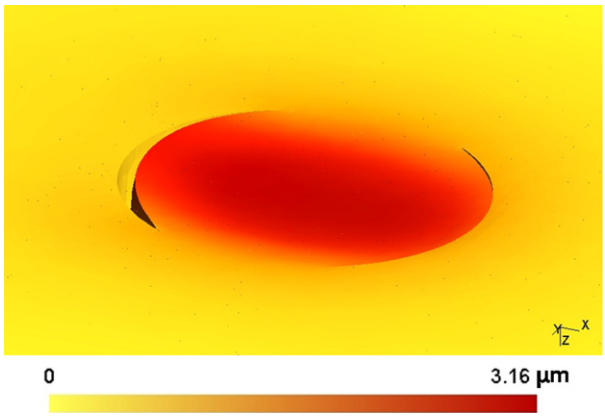

Fig. 21. Amplified representation of displacement field $\mathbf{U}(\times 10)$ for the maximum tangential load at $t = 1$.

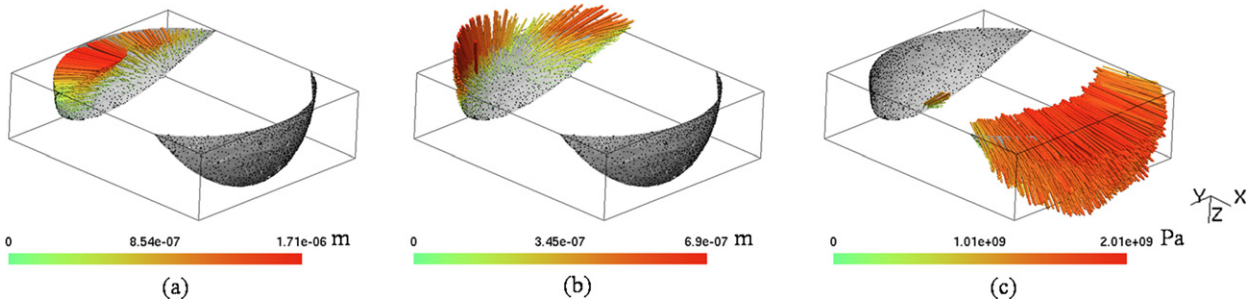

Fig. 22. (a) Relative normal displacement field at crack interface $[\mathbf{W}_N(t)] = \mathbf{W}_N^+(t) - \mathbf{W}_N^-(t)$; (b) Relative tangential displacement field at crack interface $[\mathbf{W}_T(t)] = \mathbf{W}_T^+(t) - \mathbf{W}_T^-(t)$; (c) Local traction field $\mathbf{T}(t)$ at $t = 1$.

are similar to those of the experimental cracks observed. This result emphasizes a good qualitative agreement between the prediction and the experimental observations, both on the crack locations and shapes.

Step 4: 3D fretting crack modeling. A parallelepipedic steel domain is considered with dimensions (25 mm × 16 mm × 4 mm) and mechanical properties identical to the experimental ones (see Table 2). The time-discretized two-body contact solution, i.e. pressure $p(x, y)$ and traction $q(x, y, t)$ distributions defined in step 2, is used as an input data in the X-FEM crack model. 25 time steps are used to describe the fretting cycle, cf. Fig. 17(b). A positive value of the tangential force Q acts on the x direction. These pressure and traction distributions are interpolated on "load set" surfaces relying on the finite element mesh. This technique has been detailed previously [27] and is not recalled here for succinctness. The mesh of the sample (46 266 tetrahedra) is thus locally refined on the upper surface, cf. Fig. 20(a), to provide an accurate definition of the experimental fretting loading.

Dirichlet boundary conditions $u_Z = 0$ are imposed on the bottom surface and rigid body displacements are blocked. The shapes of the two symmetrical cracks are defined on the basis of the experimental observations, cf. Fig. 15(b). These are qualitatively represented using level sets, cf. Fig. 20(b). Their surface-breaking length and maximum depth are equal to 298 µm and 95 µm respectively. They are located at $x = -171$ µm (crack 1) and $x = 171$ µm (crack 2). The crack interfaces are discretized using the global–local method. The critical size set for 2D interface element edges is $l_C = 14$ µm, leading to a distribution of 902 Gauss points per crack, cf. Fig. 20(b).

The non-linear frictional contact conditions along the crack faces inducing hysteresis phenomena, the discretized local contact fields $\mathbf{W}(t)$ and $\mathbf{T}(t)$ at each time step t are initialized with the values computed at the previous load-step $t - 1$. The approximation of the solution is computed at a level of accuracy of 10^{-4} according to the local convergence criterion developed [23].

Complex sequences of frictional contact states occur along both crack faces during the fretting cycle simulation. Amplified representations of global displacement field $\mathbf{U}$, local relative normal displacement field $[\mathbf{W}_N(t)] = \mathbf{W}_N^+(t) - \mathbf{W}_N^-(t)$ (gap between the crack faces), local relative tangential displacement field $[\mathbf{W}_T(t)] = \mathbf{W}_T^+(t) - \mathbf{W}_T^-(t)$ (slip between the crack faces) and local traction field $\mathbf{T}(t)$ are displayed in Figs. 21 and 22 at time step $t = 1$.

As displayed on Figs. 21 and 22(a), at maximum tangential load, crack 1 is opened while crack 2 is closed. Mode I, II and III stress intensity factors are computed along both crack fronts according to Eq. (17) and are displayed in Fig. 23. It is observed that mode I is predominant. Note that a ratio of nearly 10 holds between K_I and K_{II} values.

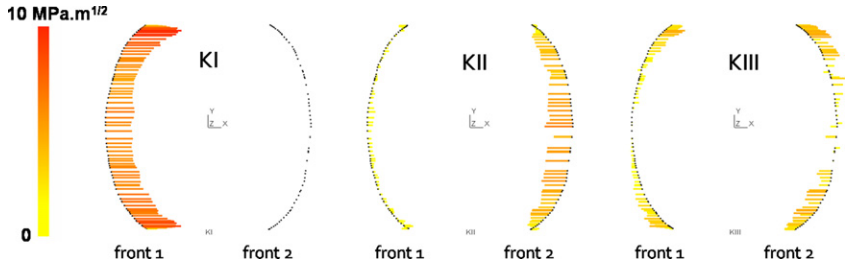

Fig. 23. Stress intensity factors K_I, K_{II} and K_{III} along the crack fronts for the maximum tangential load at $t = 1$, represented in plane (x, y).

The next step consists in combining experimental and numerical simulations at different number of cycles with corresponding crack fronts in order to formulate a specific crack growth law and to achieve fatigue life prediction. Fatigue tests are in progress.

4. Conclusion

A methodology aiming at understanding and predicting crack initiation, formation and possible self-arrest is proposed in this article based on the development of a 3D fatigue crack model.

This 3D quasi-static fatigue crack model allows dealing with frictional contact at the crack interface during complex cyclic fatigue loadings. It rests on key techniques, like the combination of the extended finite element technique with the level set technique, a global–local strategy resting on the cracked problem partition in two, a three-field weak formulation for the frictional contact problem and a dedicated Non-Locking LATIN solver (NLLA) avoiding spurious oscillations in the contact tractions when sliding is important. Numerical examples exhibiting the model robustness, accuracy and stability have been presented.

The application of this procedure to a 3D fretting fatigue test is then presented. An actual sphere/plate fretting test conducted under partial slip regime and inducing crack initiation and propagation is performed. Fretting loops are monitored and analyzed, the morphology of the two main cracks is microscopically examined using successive parallel cross sections. Input data for the numerical procedure are defined from the experimental data. The local friction coefficient at the sphere/plate contact is quantified from recorded loading conditions during the fretting cycles. Pressure and cyclic tangential tractions are then computed. The definition of the 3D crack shapes is then performed from the metallographic cross sections and the 3D crack geometry reconstruction is achieved. Level set crack surfaces and fronts are then described accordingly. NLLA-X-FEM simulations are then conducted based on the actual crack shapes. The sequences of frictional contact states at the crack interfaces are computed and mode I, II and III stress intensity factors computation is then achieved at the crack front.

The next step is to deal with fatigue crack growth behavior. Fretting tests will be conducted at different number of cycles to get representative data in terms of crack front evolution versus the number of cycles. Combining these data with the NLLA-X-FEM model will allow us to propose a fatigue crack growth law.

Acknowledgement

The support of SKF is gratefully acknowledged.

References

[1] C. Ruiz, P.H.B. Boddington, K.C. Chen, An investigation of fatigue and fretting in a dovetail joint, Exp. Mech. 24 (3) (1984) 208–217.
[2] K. Dang Van, Macro–micro approach in high cycle multiaxial fatigue, in: D.L. Mc Dowell, R. Ellis (Eds.), Advances in Multiaxial Fatigue, in: ASTM STP, vol. 1191, 1993.
[3] V. Lamacq, M.-C. Dubourg, Modelling of initial fatigue crack growth and crack branching under fretting conditions, Fatigue Fract. Eng. Mat. Struct. 22 (6) (1999) 535–542.
[4] M. Comninou, The interface crack, ASME J. Appl. Mech. 44 (1977) 631–636.
[5] D.A. Hills, M. Comninou, An analysis of fretting fatigue cracks during loading phase, Int. J. Solids Struct. 21 (4) (1985) 399–410.
[6] M.C. Dubourg, B. Villechaise, Unilateral contact analysis of a crack with friction, European J. Mech. A/Solids 8 (4) (1989) 309–319.
[7] M.C. Dubourg, B. Villechaise, Analysis of multiple fatigue cracks. Part I: theory, ASME J. Tribol. 114 (1992) 455–461.
[8] J. Melenk, I. Babuška, The partition of unity finite element method: Basic theory and applications, Comput. Meth. Appl. Mech. Eng. 39 (1996) 289–314.
[9] N. Moës, J. Dolbow, T. Belytschko, A finite element method for crack growth without remeshing, Int. J. Numer. Methods Eng. 46 (1999) 131–150.
[10] N. Sukumar, N. Moës, B. Moran, T. Belytschko, Extended finite element method for three-dimensional crack modelling, Int. J. Numer. Methods Eng. 48 (11) (2000) 1549–1570.
[11] N. Sukumar, D.L. Chopp, E. Béchet, N. Moës, Three-dimensional non-planar crack growth by a coupled extended finite element and fast marching method, Int. J. Numer. Methods Eng. 76 (5) (2008) 727–748.
[12] N. Moës, A. Gravouil, T. Belytschko, Non-planar 3D crack growth with the extended finite element and level sets – Part 1: Mechanical model, Int. J. Numer. Methods Eng. 53 (11) (2002) 2549–2568.
[13] A. Gravouil, N. Moës, T. Belytschko, Non-planar 3D crack growth with the extended finite element and level sets – Part 2: Level set update, Int. J. Numer. Methods Eng. 53 (11) (2002) 2569–2586.

[14] J. Rannou, A. Gravouil, M.C. Baietto Dubourg, A local multigrid X-FEM strategy for 3-D crack propagation, Int. J. Numer. Methods Eng. 77 (2008) 1641–1669.
[15] J. Dolbow, N. Moës, T. Belytschko, An extended finite element method for modelling crack growth with frictional contact, Comput. Meth. Appl. Mech. Eng. 53 (2001) 6825–6846.
[16] T. Elguedj, A. Gravouil, A. Combescure, A mixed augmented Lagrangian-extended finite element method for modelling elastic–plastic fatigue crack growth with unilateral contact, Int. J. Numer. Methods Eng. 71 (2007) 1569–1597.
[17] E. Vitali, D.J. Benson, Contact with friction in multi-material arbitrary Lagrangian–Eulerian formulations using X-FEM, Int. J. Numer. Methods Eng. 76 (6) (2008) 893–921.
[18] F. Liu, R.I. Borja, A contact algorithm for frictional crack propagation with the extended finite element method, Int. J. Numer. Methods Eng. 76 (10) (2008) 1489–1512.
[19] E. Béchet, N. Moës, B. Wohlmuth, A stable Lagrange multiplier space for stiff interface conditions within the extended finite element method, Int. J. Numer. Methods Eng. 78 (2009) 931–954.
[20] S. Géniaut, P. Massin, N. Moës, A stable 3D contact formulation for cracks using X-FEM, European J. Comput. Mech. 16 (1) (2007) 259–276.
[21] M. Siavelis, P. Massin, M.L. E Guiton, S. Mazet, N. Moës, Robust implementation of contact under friction and large sliding with the eXtended Finite Element Method, Eur. J. Comput. Mech. (2010).
[22] E. Pierres, M.C. Baietto, A. Gravouil, A two-scale eXtended finite element method for modeling 3D crack growth with interfacial contact, Int. J. Numer. Methods Eng. 199 (17–20) (2010) 1165–1177.
[23] R. Ribeaucourt, M.C. Baietto Dubourg, A. Gravouil, A new fatigue frictional contact crack propagation model with the coupled X-FEM/LATIN method, Comput. Meth. Appl. Mech. Eng. 196 (2007) 3230–3247.
[24] E. Giner, N. Sukumar, F.D. Denia, F.J. Fuenmayor, Extended finite element method for fretting fatigue crack propagation, Int. J. Solids Struct. 45 (22–23) (2008) 5675–5687.
[25] E. Giner, M. Tur, A. Vercher, F.J. Fuenmayor, Numerical modelling of crack-contact interaction in 2D incomplete fretting contacts using X-FEM, Tribology International 42 (2009) 1269–1275.
[26] E. Giner, M. Tur, J.E. Tarancón, F.J. Fuenmayor, Crack face contact in X-FEM using a segment-to-segment approach, Int. J. Numer. Methods Eng. (2009), online.
[27] M.C. Baietto, E. Pierres, A. Gravouil, A multi-model X-FEM strategy dedicated to frictional crack growth under cyclic fretting fatigue loadings, Int. J. Solids Struct. 47 (10) (2010) 1405–1423.
[28] D. Dureisseix, H. Bavestello, Information transfer between incompatible finite element meshes: Application to coupled thermo-viscoelasticity, Comput. Meth. Appl. Mech. Eng. 195 (2006) 6523–6541.
[29] P. Ladevèze, Nonlinear Computational Structural Mechanics, Springer, New York, 1998.
[30] L. Champaney, Modular analysis of assemblages of three-dimensional structures with unilateral contact conditions, Comput. Struct. 73 (1999) 249–266.
[31] N. Moës, B. Béchet, M. Tourbier, Imposing Dirichlet boundary conditions in the extended finite element method, Int. J. Numer. Methods Eng. 67 (2006) 1641–1669.
[32] A. Hansbo, P. Hansbo, A finite element method for the simulation of strong and weak discontinuities in solid mechanics, Comput. Meth. Appl. Mech. Eng. 193 (2004) 3523–3540.
[33] R. Becker, E. Burman, P. Hansbo, A Nitsche extended finite element method for incompressible elasticity with discontinuous modulus of elasticity, Comput. Meth. Appl. Mech. Eng. 198 (2009) 3352–3360.
[34] I. Nistor, M.L.E. Guiton, P. Massin, N. Moës, S. Géniaut, An X-FEM approach for large sliding contact along discontinuities, Int. J. Numer. Methods Eng. 78 (12) (2008) 1407–1435.
[35] M. Duflot, A study of the representation of cracks with level sets, Int. J. Numer. Methods Eng. 70 (11) (2006) 1261–1302.
[36] M. Gosz, J. Dolbow, B. Moran, Domain integral formulation for stress intensity factor computation along curved three-dimensional interface cracks, Int. J. Solids Struct. 35 (1998) 1763–1783.
[37] M. Gosz, B. Moran, An interaction energy integral method for computation of mixed-mode stress intensity factors along non-planar crack fronts in three dimensions, Eng. Fract. Mech. 69 (3) (2002) 299–319.
[38] H. Rajaram, S. Socrate, D.M. Parks, Application of domain integral methods using tetrahedral elements to the determination of stress intensity factors, Eng. Fract. Mech. 66 (5) (2000) 455–482.
[39] T. Nakamura, D.M. Parks, Determination of elastic T-stress along three-dimensional crack fronts using an interaction integral, Int. J. Solids Struct. 29 (13) (1992) 1597–1611.
[40] B.N. Rao, S. Rahman, An enriched meshless method for non-linear fracture mechanics, Int. J. Numer. Methods Eng. 59 (2004) 197–223.
[41] J. Johnson, J. Qu, An interaction integral method for computing mixed mode stress intensity factors for curved bimaterial interface cracks in non-uniform temperature fields, Eng. Fract. Mech. 74 (2007) 2282–2291.
[42] A. Dorogoy, L. Banks-Sills, Shear loaded interface crack under the influence of friction: a finite difference solution, Int. J. Numer. Methods Eng. 59 (13) (2004) 1749–1780.
[43] B. Moran, C.F. Shih, Crack tip and associated domain integrals from momentum and energy balance, Eng. Fract. Mech. 27 (6) (1987) 615–642.
[44] P.A. Guidault, O. Allix, L. Champaney, C. Cornuault, A multiscale extended finite element method for crack propagation, Comput. Meth. Appl. Mech. Eng. 197 (2008) 381–399.
[45] P. Laborde, Y. Renard, Fixed point strategies for elastostatic frictional contact problems, Math. Methods Appl. Sci. 31 (4) (2008) 415–441.
[46] P. Blanchard, C. Colombier, V. Pellerin, S. Fayeulle, L. Vincent, Material effect in fretting wear: iron, titanium and aluminium alloys, Metallurgical Transaction 22 (1991) 1535–1544.
[47] L. Vincent, Y. Berthier, M. Godet, Testing methods in fretting fatigue: a critical appraisal, ASTM 1159 (1992) 317–330.
[48] S. Fouvry, Ph. Kapsa, L. Vincent, Analysis of sliding behaviour for fretting loadings; determination of transition criteria, Wear 185 (1995) 35–46.
[49] R.D. Mindlin, H. Deresiewicz, Elastic spheres in contact under varying oblique forces, ASME J. Appl. Mech. E 20 (1953) 327–344.
[50] X. Robin, Crack Initiation Study Under Fretting Fatigue Conditions, Master Recherche, 2006, 42 p.
[51] K.L. Johnson, Contact Mechanics, Cambridge University Press, Cambridge, 1985.
[52] S. Fouvry, Ph. Kapsa, L. Vincent, K. Dang Van, Theoretical analysis of fatigue cracking under dry friction for fretting loading conditions, Wear 195 (1996) 21–34.